Analysis of Object Taken from Patient John Smith

Report Author: Steve Colbern

25 January, 2009

Background Information

Personal History of Subject

Mr. John Smith is in his 40's, and is married with 3 children. The subject has a strong technical background, and is currently a researcher in the Materials Science field.

Case History

The subject has had a lifelong history of UFO sightings, and missing time experiences. On the night of February 28, 2008, Mr. Smith was alone in his house. About 10:30 PM, he sighted two unusually large raccoons in the avocado tree, in his back yard. He fed the animals, and observed for them for some time. Mr. Smith then went to bed, and slept until approximately 8:00 AM the following morning.

Upon awakening, Mr. Smith noticed a burning pain in the tip of his left, second toe, and a soreness on the right side of his head. Inspection revealed two apparent puncture wounds on the underside of the end of the left, second, toe, and a scratch on its right side. One of the puncture wounds in the toe was found to fluoresce green under ultraviolet (UV) illumination.

Over the next four days, the pain in the toe increased, and felt like a strong electric shock, whenever any weight was placed on the end of the affected toe. The pain was at a maximum four days after the incident, and decreased slowly thereafter.

Mr. Smith then saw Dr. Roger Leir, who obtained X-rays of Mr. Smith's left foot. A small (~3 mm) foreign object showed up on the X-rays, under the end of the distal phalanx bone of the left, second, toe (Figure 1).

The object resembled a bent piece of wire on the X-ray. Dr. Leir commented that the object had approximately the same X-ray density as human bone.
A subsequent CAT scan of the left foot confirmed the presence of a foreign object in the same toe.

Gaussmeter, and radio frequency analyzer (RF) tests were done on the object, on August 21, 2008, by Dr. Leir, at his Thousand Oaks office, while it was still in Mr. Smith's body. These tests indicated that the object was emitting radio waves in the Gigahertz (1.2GHz), Megahertz (110MHz and 17 MHz), and Extremely Low Frequency (ELF, 8Hz) bands. The object also generated a magnetic field of > 10 mGauss.

The object in Mr. Smith's toe was removed surgically on September 6, 2008, by Dr. Roger Leir, and Dr. John Matriciano. The object was apparently brittle, and broke into 12 pieces during removal. The shape of the object was originally cylindrical, with a size (~4 mm X 1 mm dia.) and shape very similar to several objects that Dr. Leir had removed previously, from other patients (Figure 2).

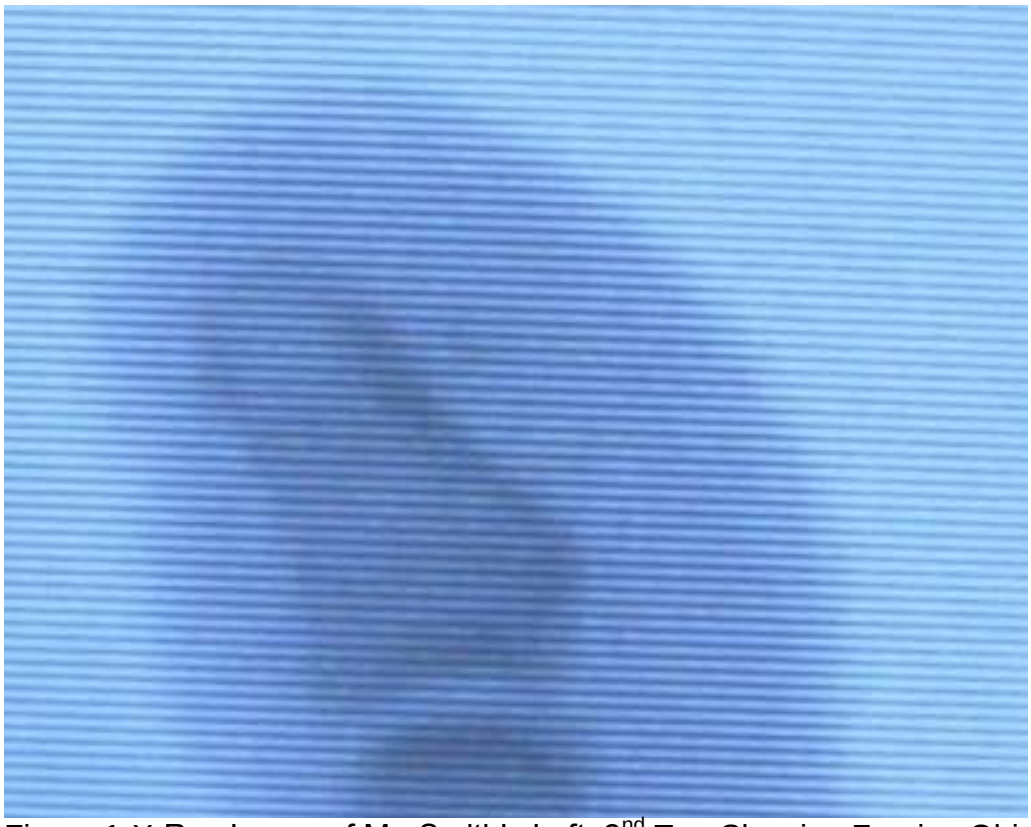

Figure 1-X-Ray Image of Mr. Smith's Left, 2nd Toe-Showing Foreign Object

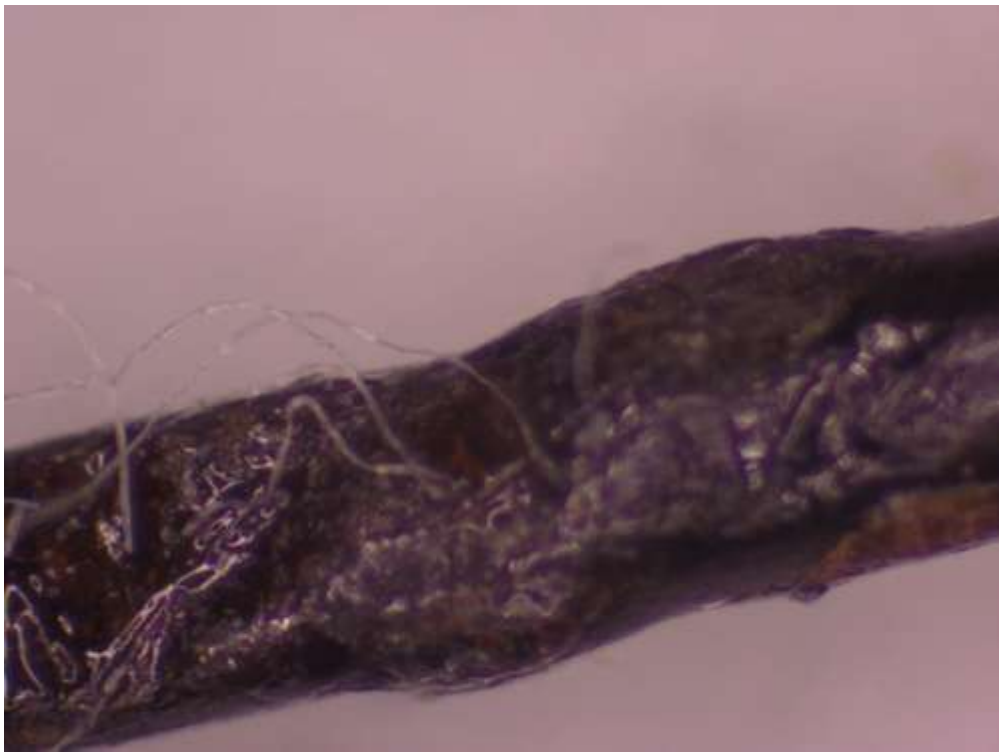

Figure 2-Implant Object Removed Intact-Similar to "John Smith" Object before removal

Pathology tests on the tissue surrounding the object showed no inflammation, or immunological reaction, by the subject's body to the presence of the object.

The pieces of the object turned black, then red, upon refrigerated storage in blood serum, taken from Mr. Smith. Within 12 hrs of removal, the pieces of the object lined up in the original order, as if trying to re-assemble.

One of the pieces of the object was given to the author of this report for analysis.
Mr. Smith stated that after the object was removed, there was a definite, but subtle change in his mood and thought processes, and that he felt more like his "old self".

Analytical Procedure

The sample was inspected with the naked eye, and then imaged under light microscopy, using an Olympus SZ-40 dissecting scope and an Olympus BH-2 microscope. Magnifications from 10X-400X were utilized.

The sample was then imaged using a JEOL 7500F scanning electron microscope (SEM). Magnifications between 150X and >100,000X were utilized. The sample was subjected to energy dispersive X-ray elemental analysis (EDX), along with the SEM imaging.

The sample was then exposed to a strong magnetic field, generated by a neodymium-iron-boron (NIB) magnet, to observe any ferromagnetic behavior.

Raman spectroscopy was also done on the sample, using a Horiba/Jovin Yvon Aramis Raman spectrometer. Both 532 nm and 633 nm laser excitation wavelengths were used.

The sample was later (26 November, 2008) sent out to an independent laboratory for more sensitive elemental analysis, using inductively coupled plasma-mass spectrometry (ICP-MS).

Analysis Results

Appearance of Sample

The sample was a small chunk of solid material, approximately cubic in shape, approximately 1 mm X 0.5 mm X 0.5 mm in dimensions, and dark, reddish in color.
The sample was delivered stored in a small, plastic, screw-top medical specimen vial, and covered in blood serum from the patient, to prevent degradation.

Light Microscopy

The sample was first imaged under the dissecting microscope, to obtain low-magnification views (10X-40X magnification) of the entire piece.
The sample was imaged both in the original container, in blood serum, and in the open air (Figures 3 and 4). Drying the sample appeared to cause no degradation. The low-magnification views of the sample revealed that the sample had a somewhat rough, and irregular, surface.

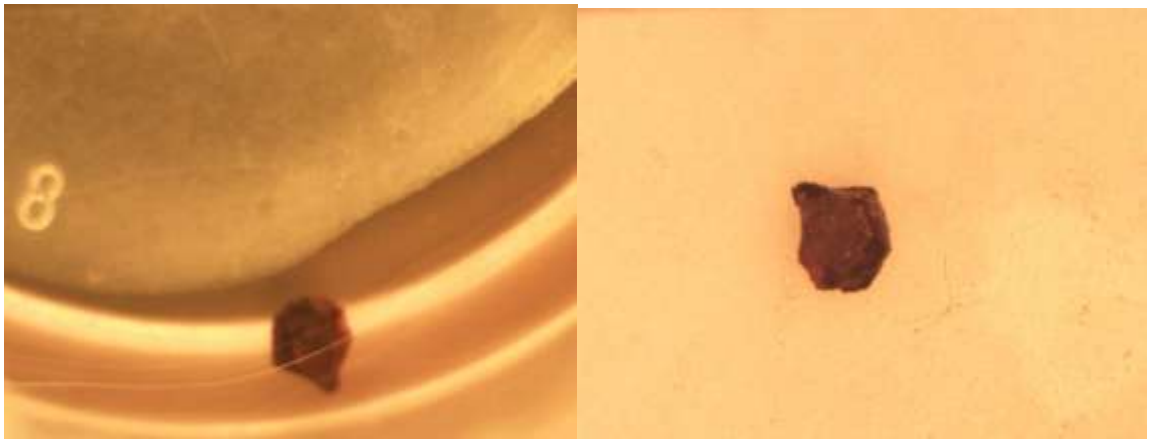

Figures 3 and 4-Sample in Blood Serum and in Air-10X Magnification

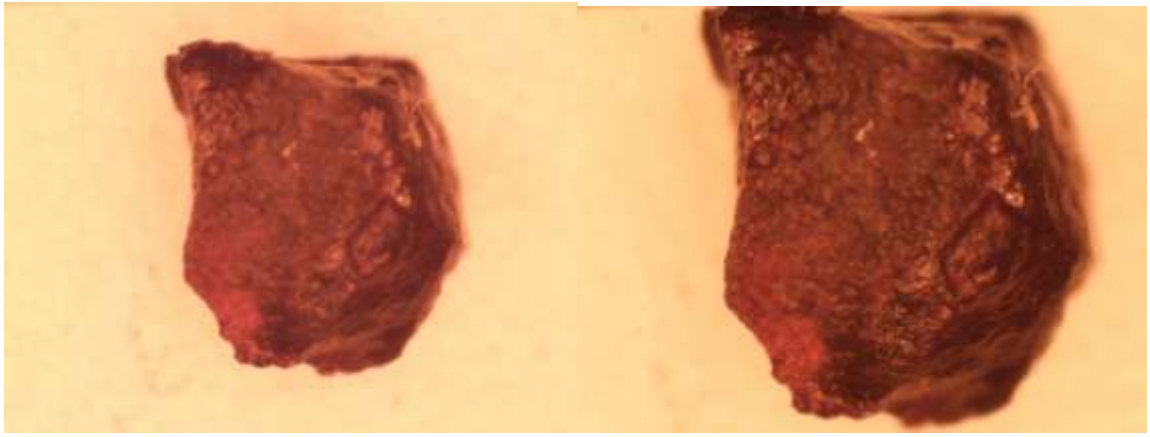

Figures 5 and 6-Sample in Air-30X and 40X Magnification

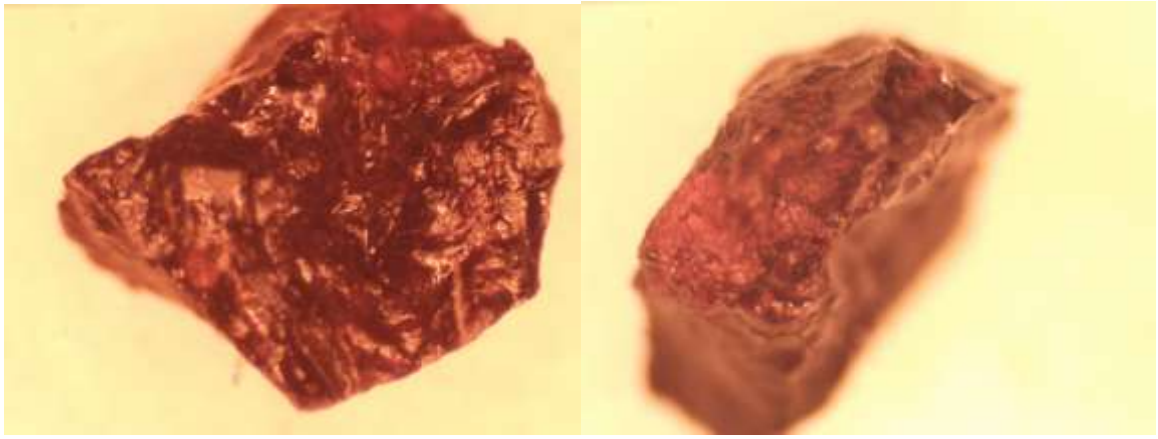

Figures 7 and 8-Sample in Air-40X Magnification

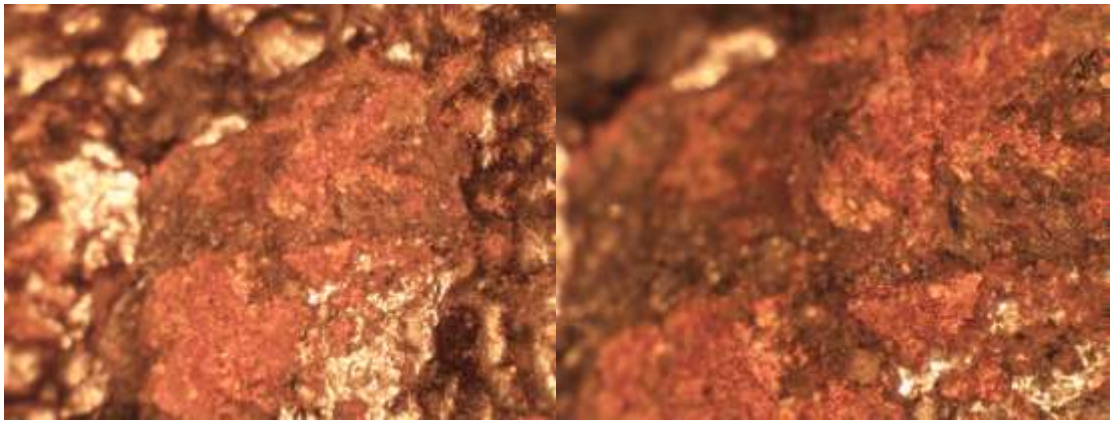

Figures 9 and 10-Fragment of Campo Del Cielo Iron Meteorite-10X and 20X

A reddish patina extended over a large percentage of the sample surface, which had a color resembling that of iron oxide (Figures 5, 6, and 8). The patina also strongly resembled the corrosion product seen on the surfaces of iron meteorites, which have been exposed to the Earth's atmosphere for some time (Figures 9 and 10).

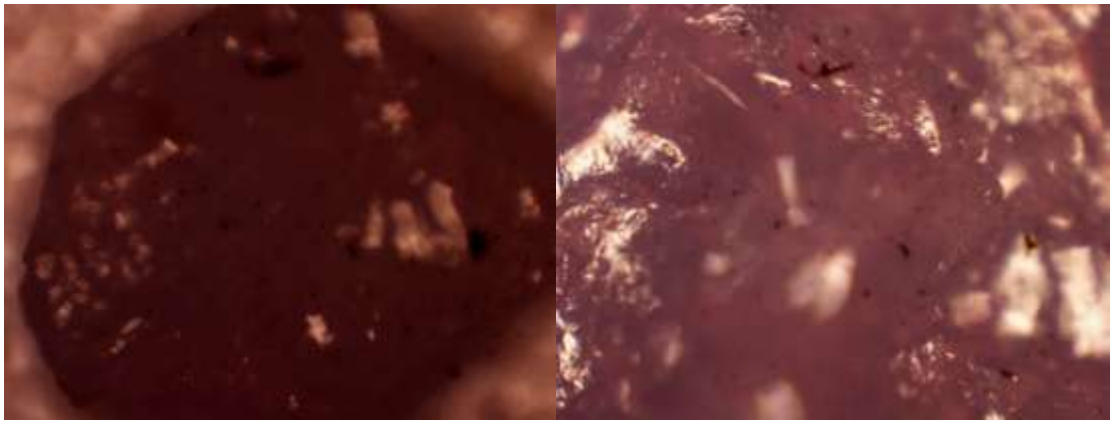

Figures 11 and 12-50X and 100X Magnification of Sample-Showing shiny surface and inclusions of white material

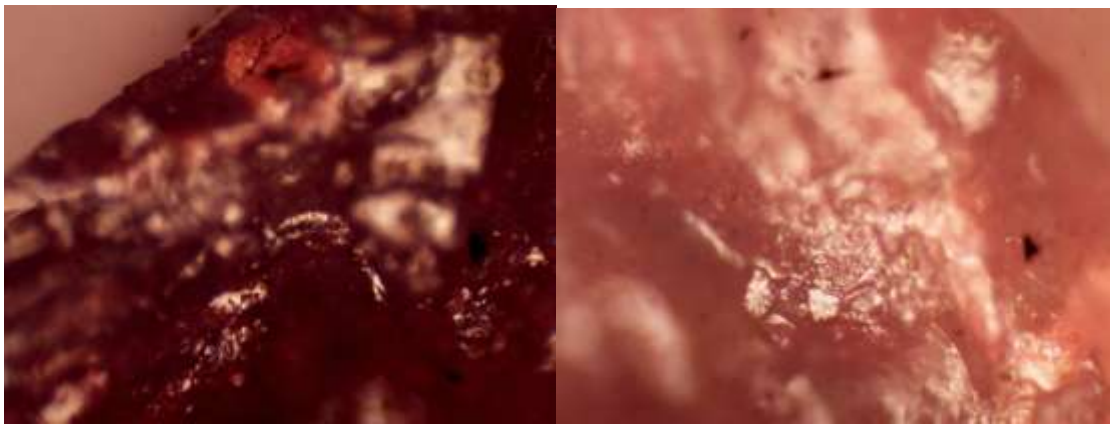

Figures 13 and 14-100X and 200X Magnification of Sample

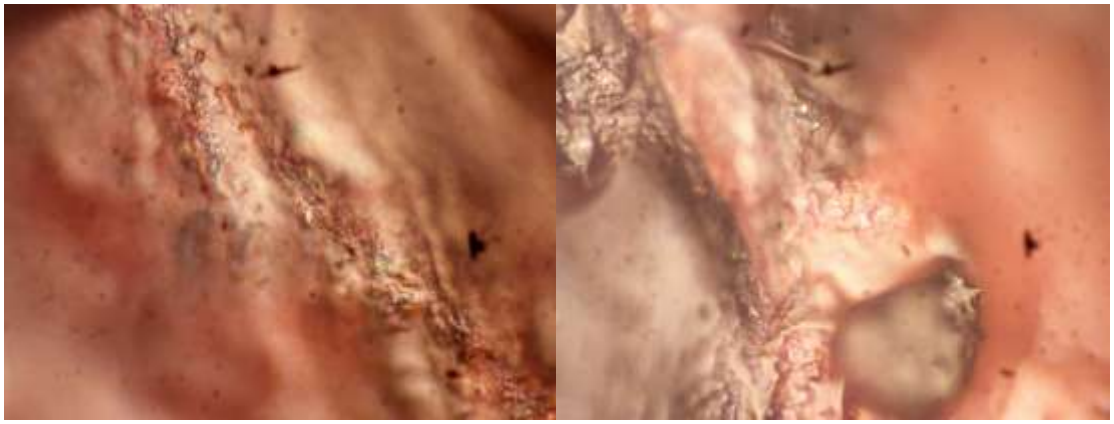

Figures 15 and 16-400X Magnification of Sample-Showing opalescence of shiny surface material

A dark, shiny, surface was also observed on the surface of one side of the sample, which remained shiny even after the sample had completely dried (Figure 6).
The sample was then placed under the high-power Olympus microscope, and images taken at 50X-400X magnification (Figures 11-16).

Under higher (50X-100X) magnification, inclusions of a light-colored material were evident on the dark, shiny side of the sample (Figures 11 and 12).
At 400X magnification, an opalescent sheen was revealed on the shiny material, which resembled that of mother-of-pearl (Figures 15 and 16).
Areas of red patina were interspersed with the areas of shiny, opalescent material.

SEM Imaging

Scanning Electron Microscope (SEM) imaging was done with gradually increasing magnification, with the first images being taken at a magnification low enough to show any bulk structure possessed by the sample (Figures 17 and 18).

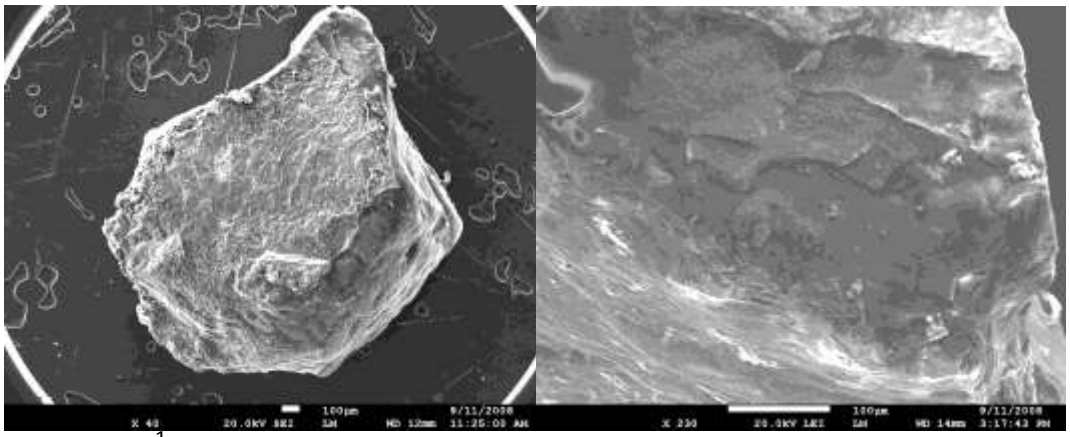

Figures 17[1] and 18-Low magnification Images of Sample (40X and 230X)-Showing whole sample and outer layer over darker bulk material

[1] Figure 15 shows the shiny sample surface, seen in light microscopy (upper sample surface in image in Figure 5).

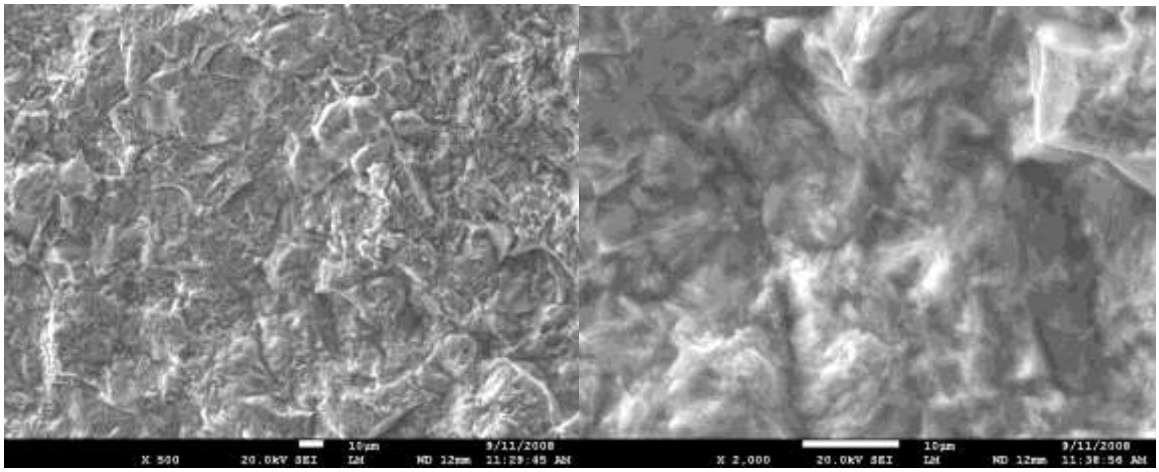

Figures 19 and 20-Higher Magnification Views of Shiny Layer of Sample (500X and 2,000X)

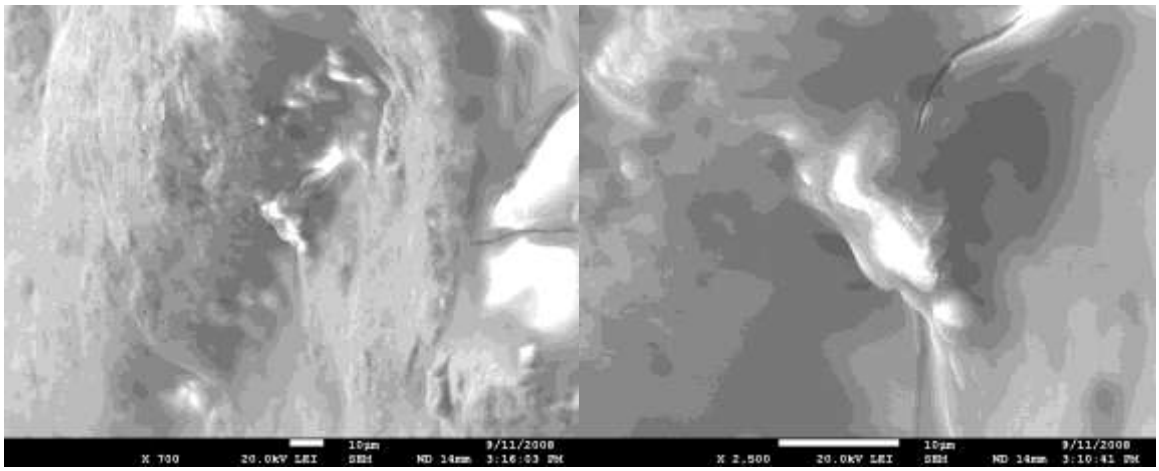

Figures 21 and 22-Higher Magnification Views of Dark, Bulk, Portion of Sample (700X and 2,500X)

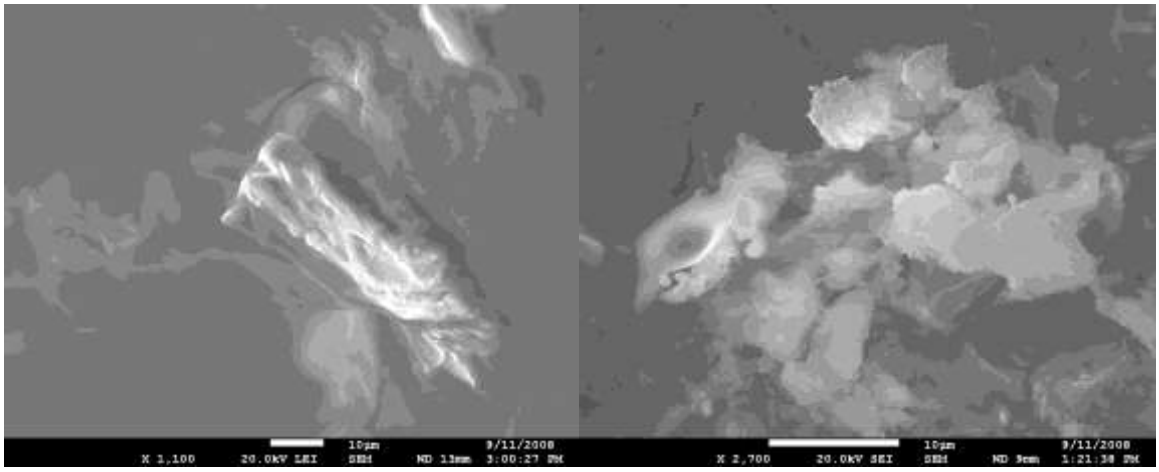

Figures 23 and 24-Inclusions of Light Material in Dark, Bulk, Area of Sample (1,100X and 2,700X)

These images showed that the shiny, opalescent, phase seen in the light microscope images appeared to represent an outer layer, or coating on the sample (Figure 18). The inner, bulk, portion of the sample consists of a darker[2] material.

The material that the outer layer of the sample was composed of was seen to be fairly rough, under 500X-2,000X magnification, with the largest surface irregularities on the order of a 5-20 microns (um) in height (Figures 19 and 20).

The darker, inner, bulk, material of the sample appeared somewhat smoother than the sample outer layer, with surface irregularities on the order of a few microns in height (Figure 21).

Some areas of the bulk material appeared quite smooth, with few surface features in evidence, other than cracks, and some light-colored areas (Figure 22).

Higher magnifications revealed that these light-colored areas resemble the material seen in the outer layer of the sample (Figures 23 and 24). Some of these inclusions of the lighter material had unusual, and complex, structures (Figures 25, 26, and 33), with sharp, horn-like, points, and long bone-like structures in evidence.

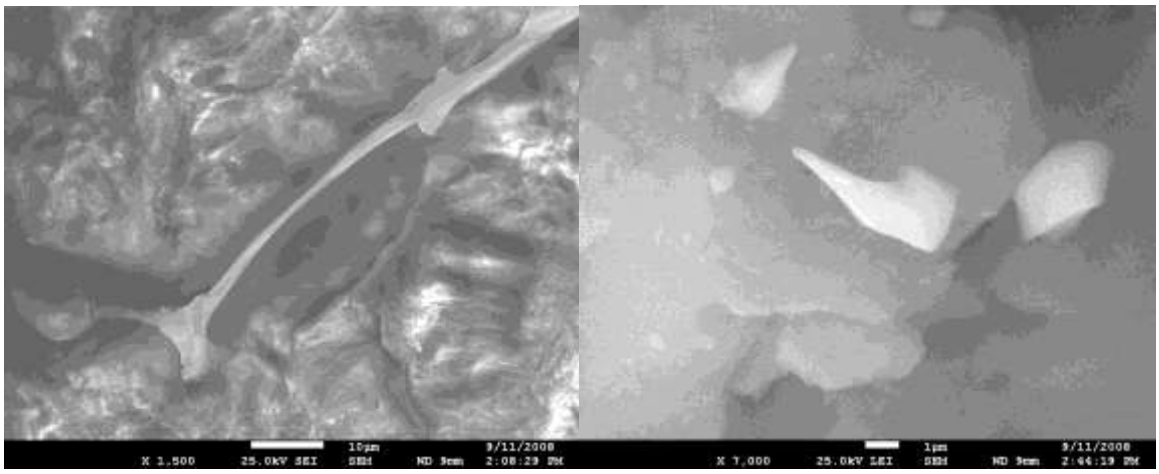

Figures 25 and 26-Views of Oddly Shaped Light Material Inclusions (1,500X and 7,000X)

[2] "Dark", in the context of SEM imaging refers to a surface which absorbs electrons efficiently. Light areas in SEM images are those which reflect electrons efficiently. In this case, the darker material, seen in SEM images, was the Fe-Ni phase (see EDX data).

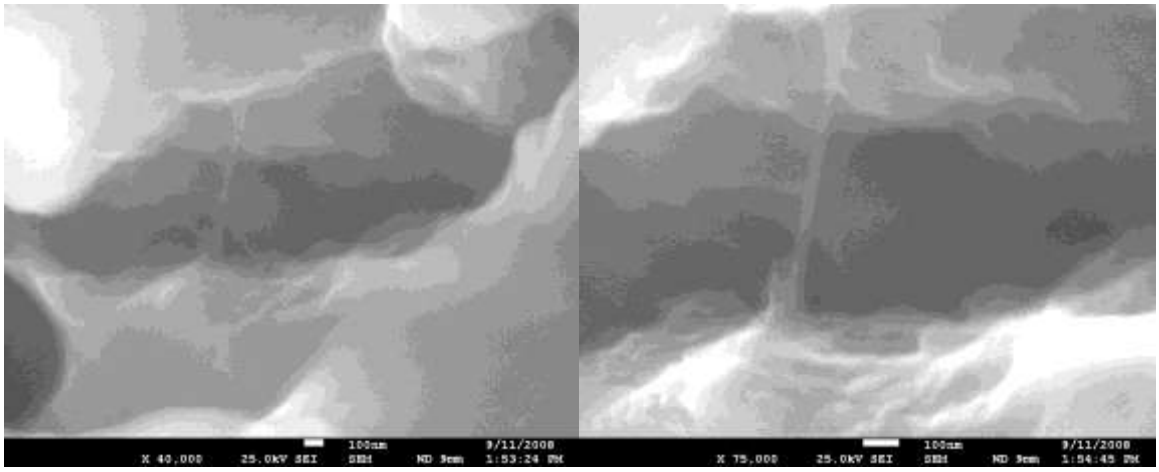

Figures 27 and 28-High Magnification Views of Cracks in Shiny Layer of Sample-Showing Nanofibers (40,000X and 75,000X)

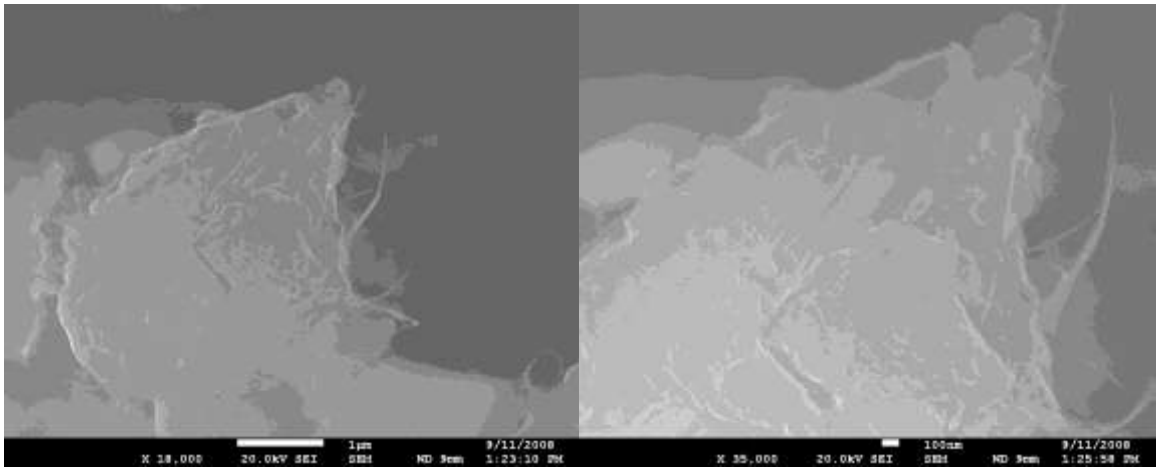

Figures 29 and 30-Higher Magnification Views of Light Material Inclusion in Dark Area of Sample-Showing Nanofibers (18,000X and 35,000X)

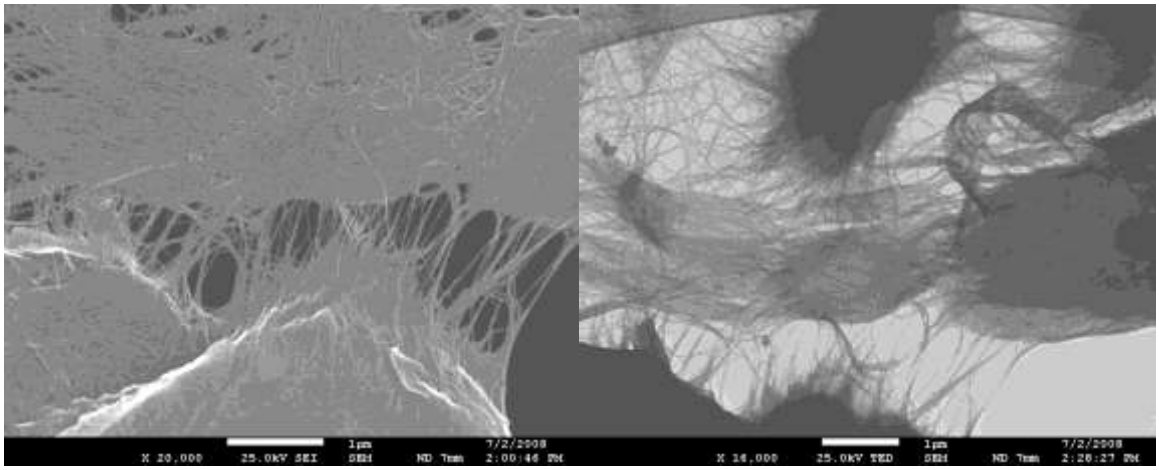

Figures 31 and 32-Single-Walled carbon Nanotubes (arc process)-Shown for Comparison

Nanofibers, with a primary bundle diameter of approximately 10 nanometers (nm) were seen in both the sample outer coating material, and in the inclusions of light material in the dark areas of the sample (Figures 27-30). These nano-fibers resemble bundles of single-walled carbon nanotubes (SWCNT, Figures 31 and 32).

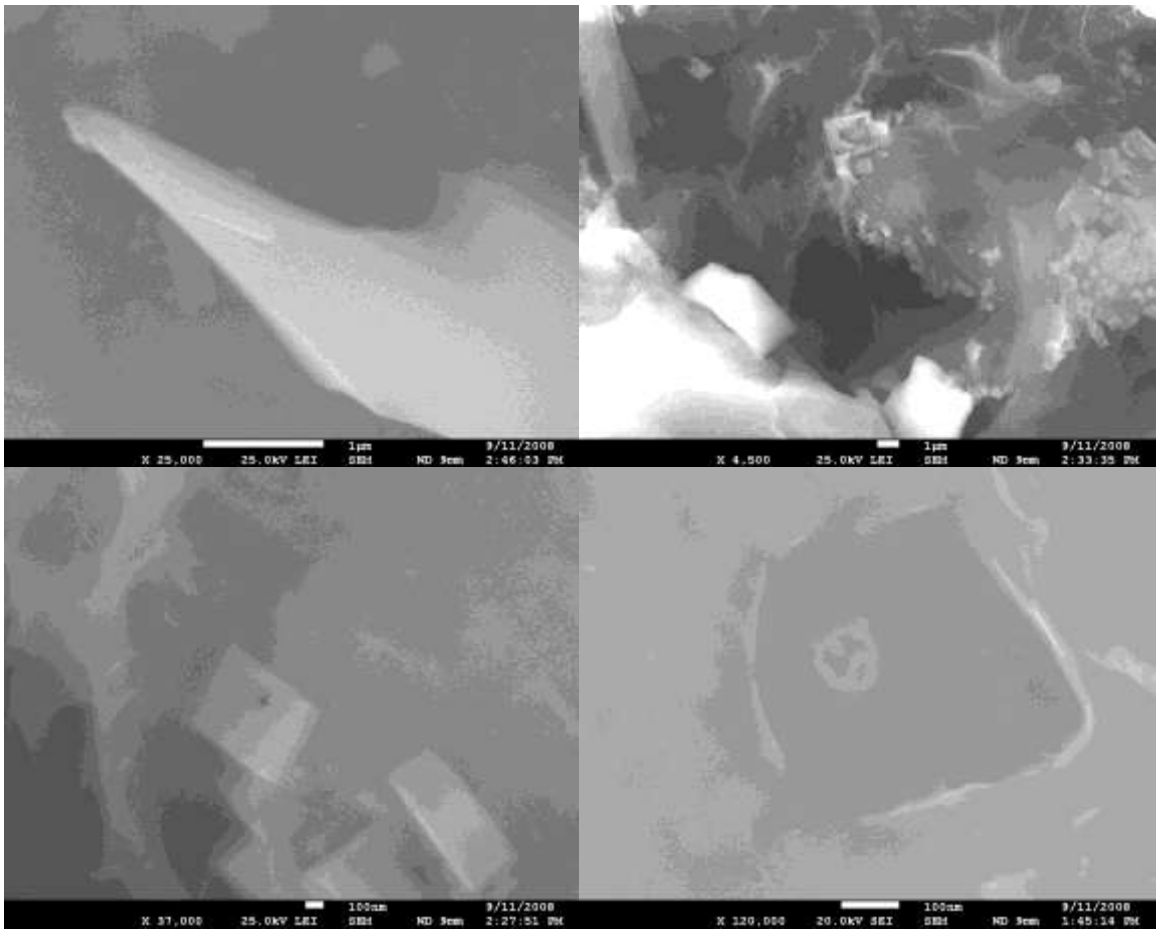

Figures 33-36-Unusual Surface Structures in Bulk Material of Sample

Highly regular crystal inclusions, and small pits, both ~500 nm in largest dimension, were also seen in the dark areas of the sample (Figures 33-36).

EDX Data

Energy Dispersive X-Ray (EDX) elemental analysis scans of a relatively large area of the sample[3] (500X magnification) revealed that the object is composed mainly of oxygen, iron, nickel, carbon, and silicon.

[3] The sample was labeled "Sun Nano Impurity", in the EDX data, for security reasons.

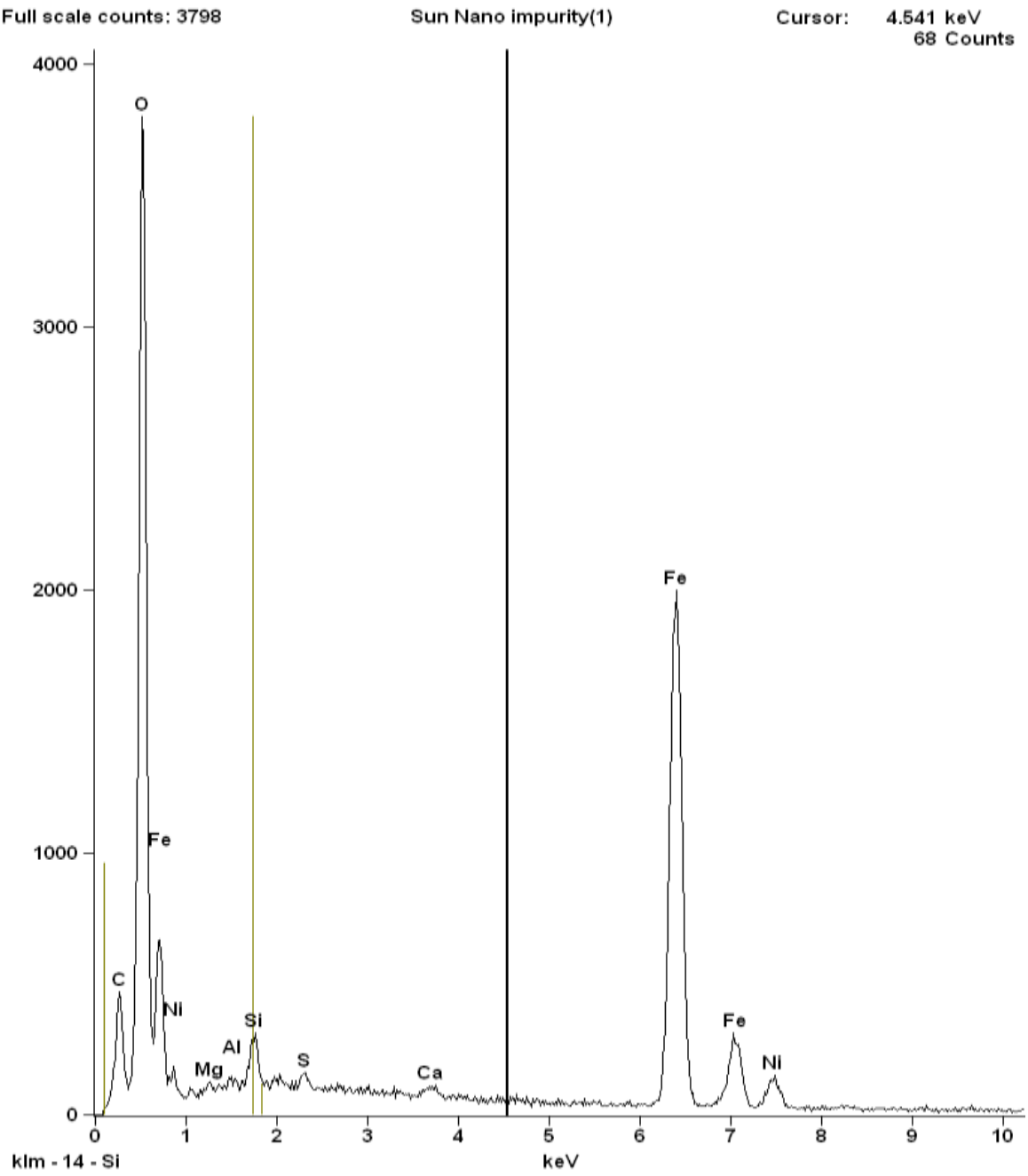

Figure 37-Large-Area EDX Scan of Object

Smaller amounts of magnesium, aluminum, calcium, and sulfur, phosphorus, and sodium also showed up in the initial EDX scans (Figures 37 and 38).

The small-area EDX scan (point and shoot technique), in which the elemental composition of a very small area in an SEM image is analyzed, was used to determine that the darker areas of the sample are composed mainly of iron and nickel, with a high content of carbon and oxygen.

Small amounts of silicon, along with traces of sodium, magnesium, aluminum, phosphorus, sulfur, chlorine, calcium, were also present in the dark material (Figures 39, 40, 43, 44, and 48). The EDX instrument software also detected traces of tungsten, and iridium (not shown).

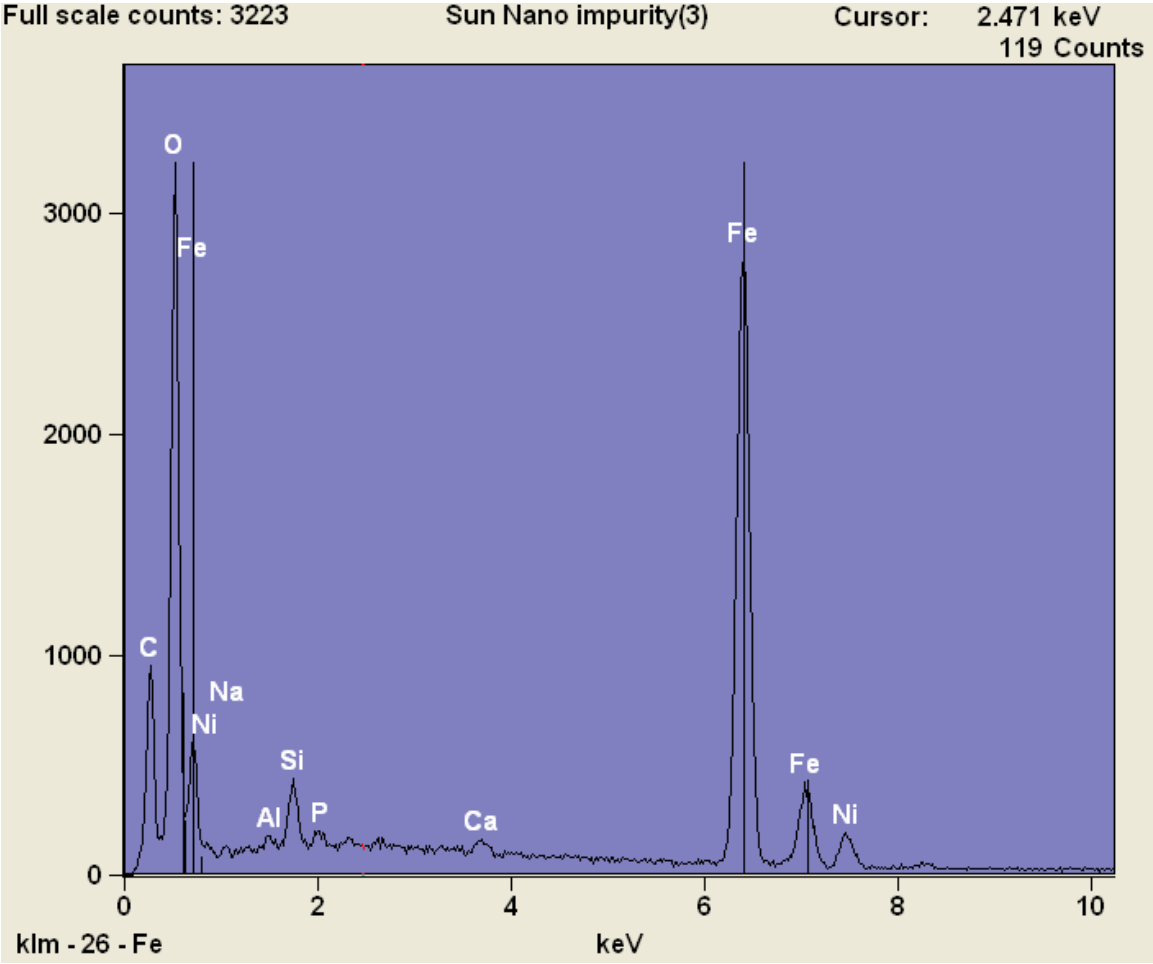

Figure 38-Second Large-Area EDX Scan of Object

The Fe/Ni peak height ratio data was used to calculate the percentage of nickel[4] in the Fe-Ni phase of the sample. The concentration of nickel was found to be 5 wt. %-6 wt. % with respect to the mass of the Fe-Ni sample phase.

The lighter areas of the sample are composed mainly of carbon, oxygen, silicon, sulfur, aluminum, calcium, iron and nickel, with smaller amounts of sodium, phosphorus, chlorine, potassium, and titanium (Figures 39-42, and 44-45).

Much lower amounts of iron and nickel were detected in the light areas of the sample than in the dark areas.

[4] Calculated as Ni peak height/(Fe peak height + Ni peak height)

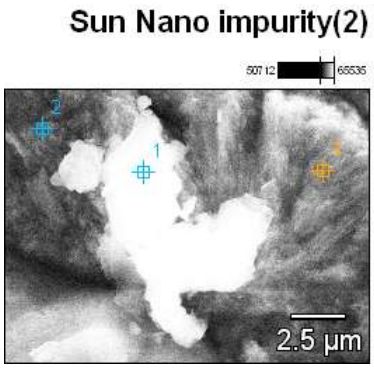

Image Name:
Sun Nano impurity(2)
Accelerating Voltage: 20.0 kV
Magnification: 7000

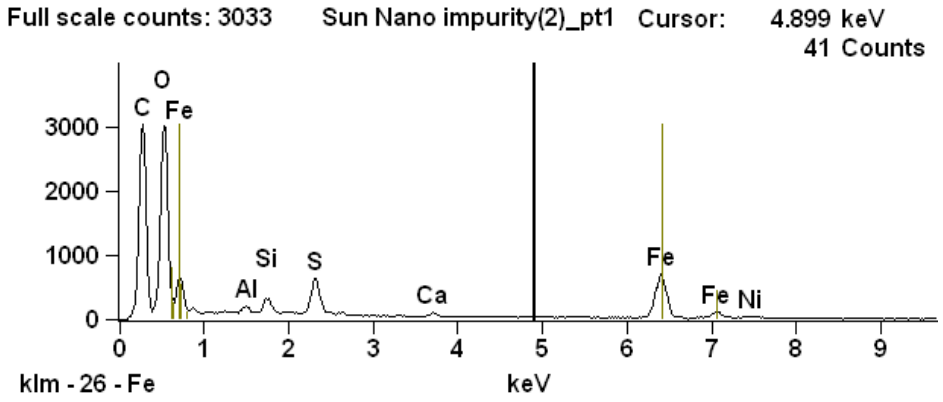

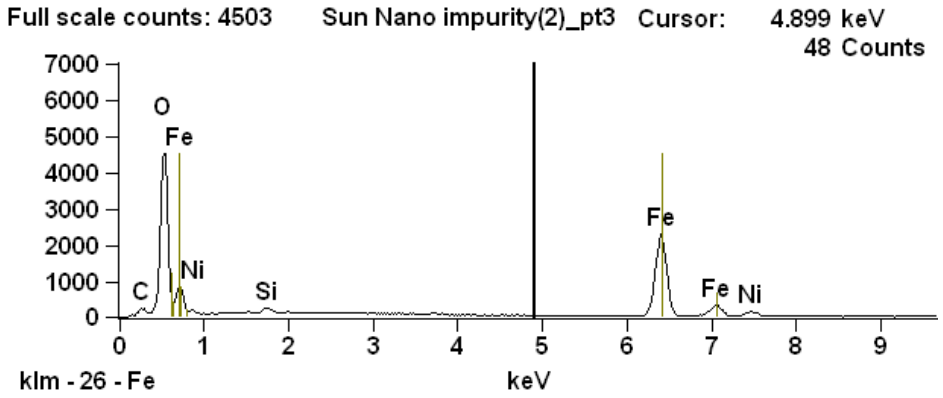

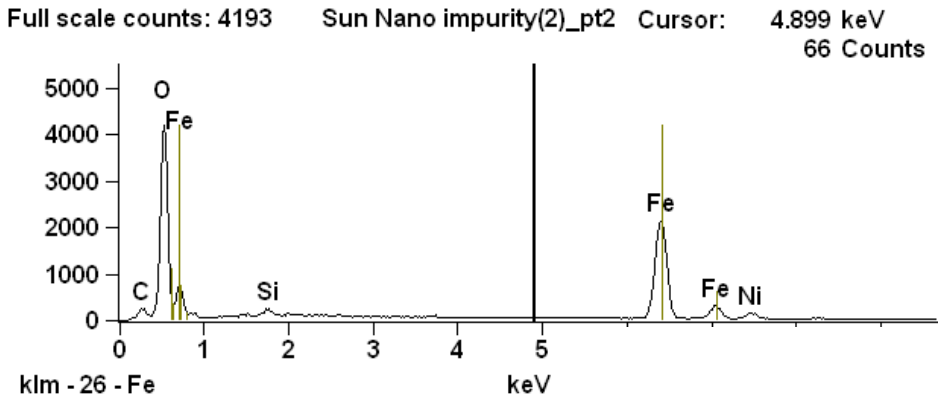

Figure 39-Small Area EDX Scan of Light

Image Name:
Sun Nano impurity(4)

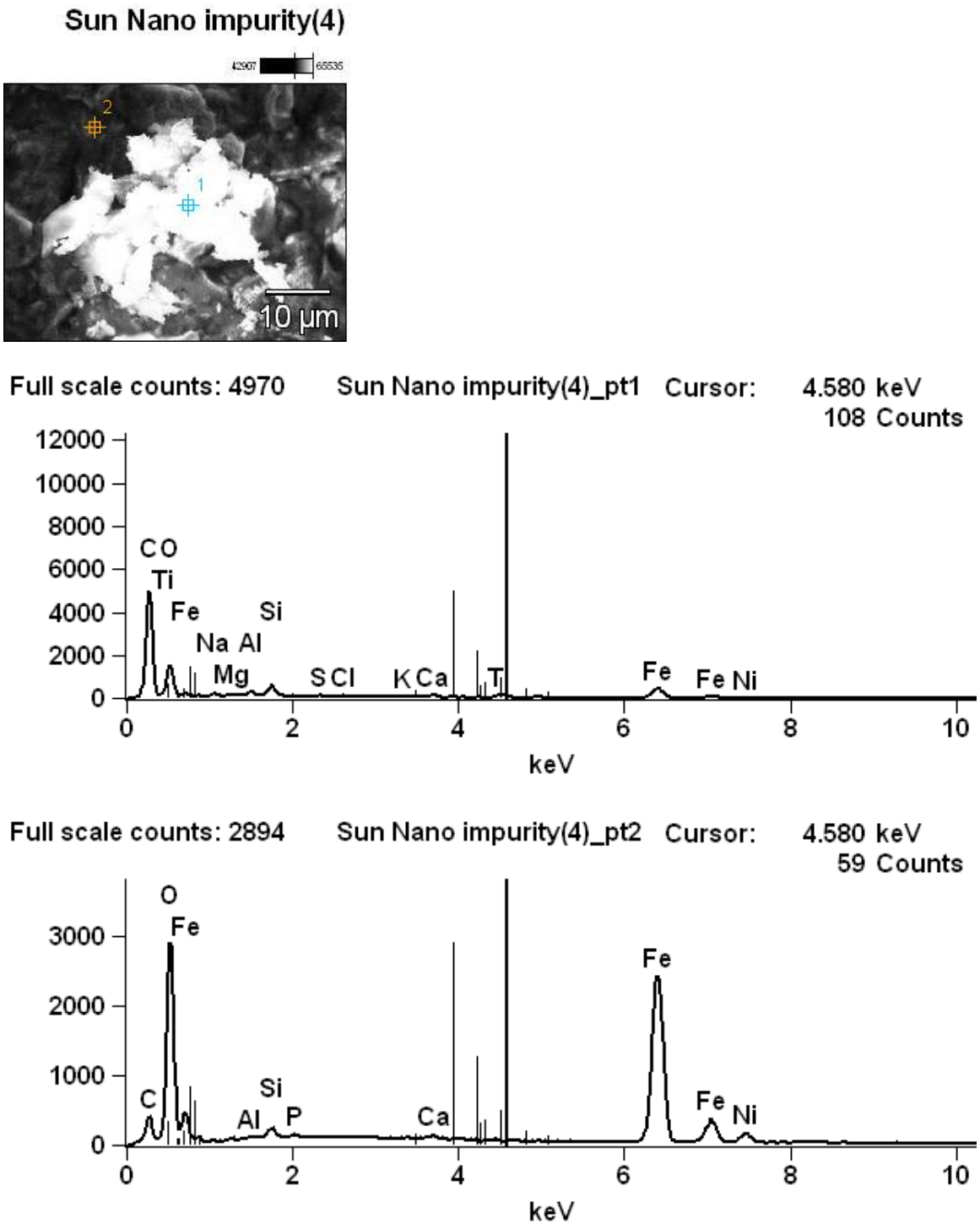

Figure 40- Small Area EDX Scan of Light and Dark Areas of the Sample

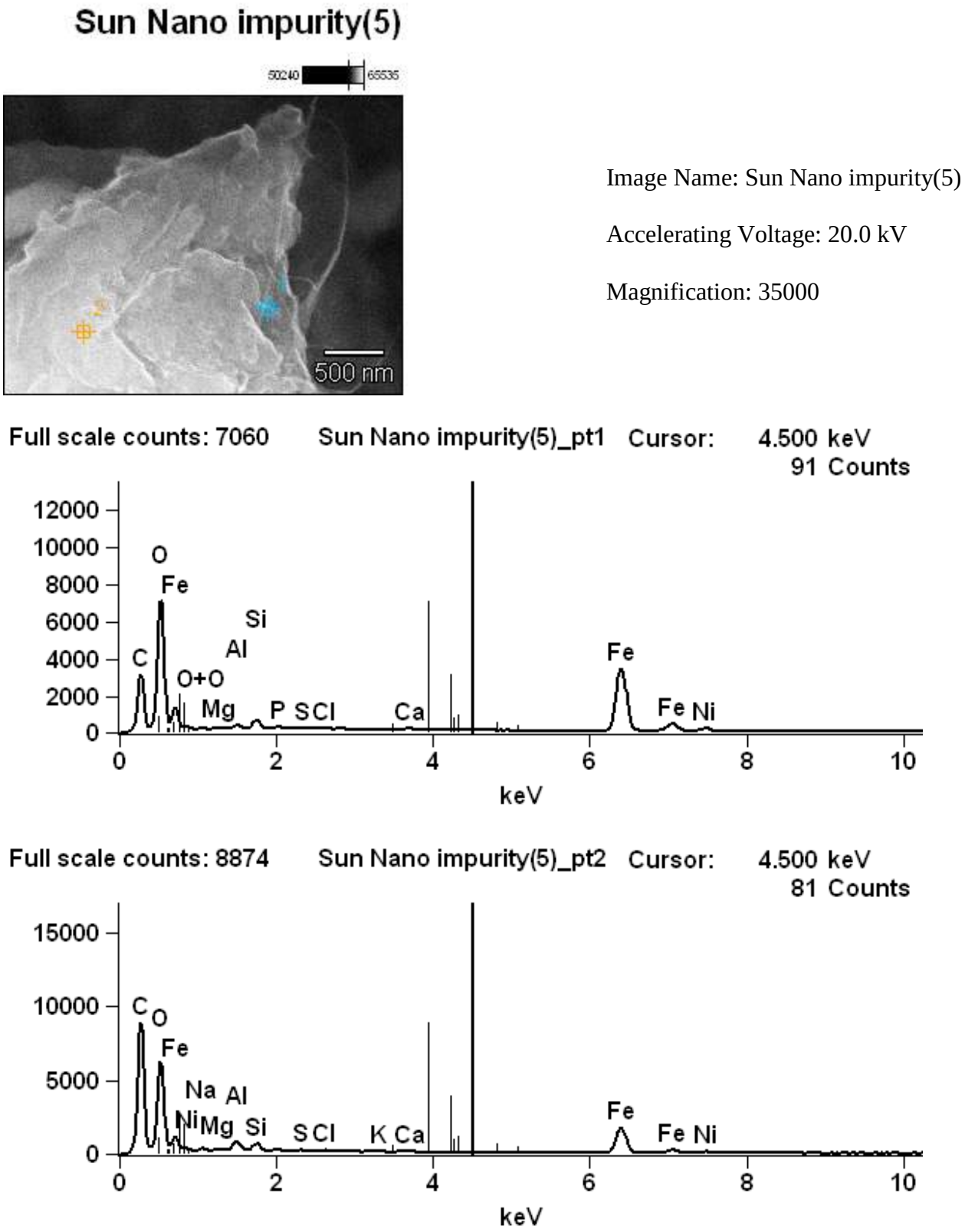

Figure 41- Small Area EDX Scan of Light Area of the Sample-Showing Nanotube Bundles

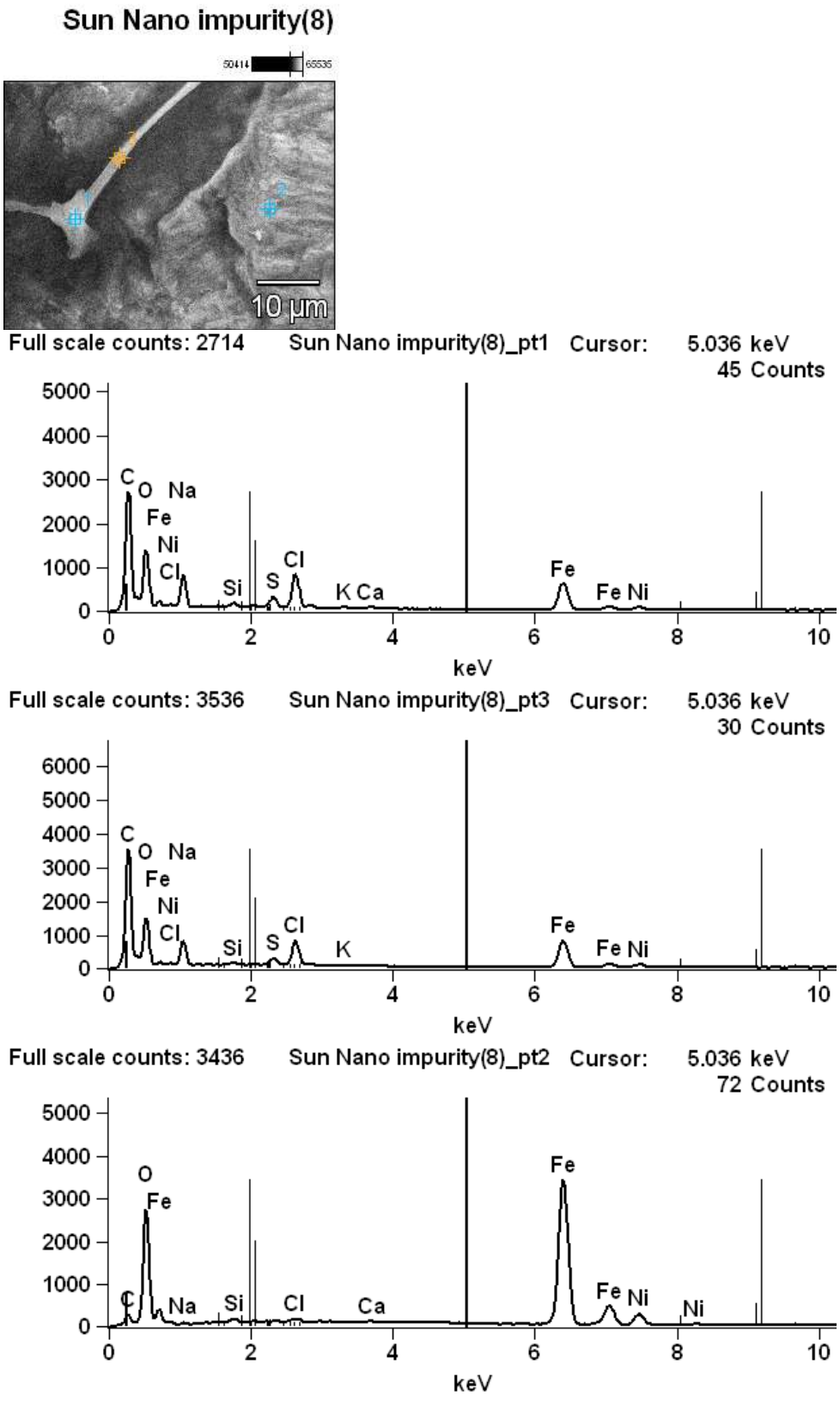

Figure 42- Small Area EDX Scan of Light Area of the Sample-Showing Bone-like Structure

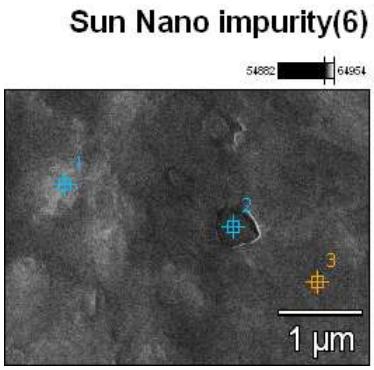

Image Name: Sun Nano impurity(6)

Accelerating Voltage: 20.0 kV

Magnification: 27000

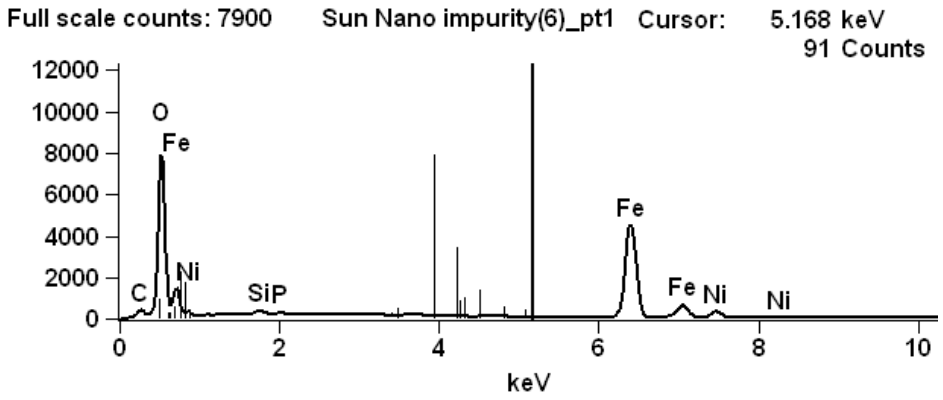

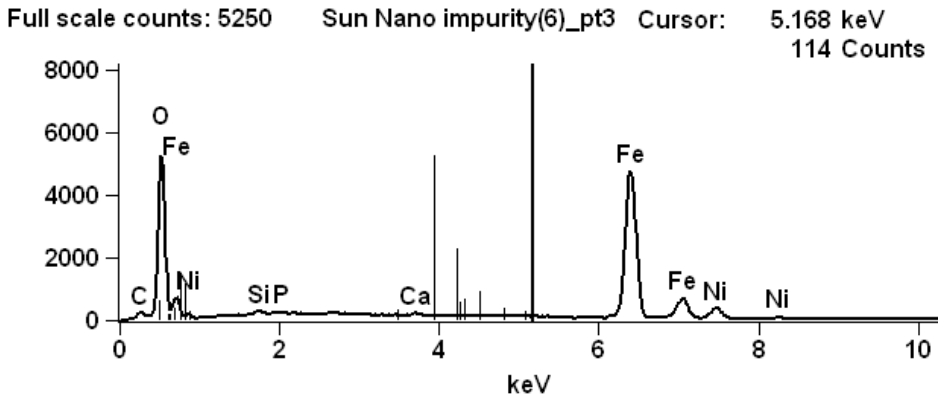

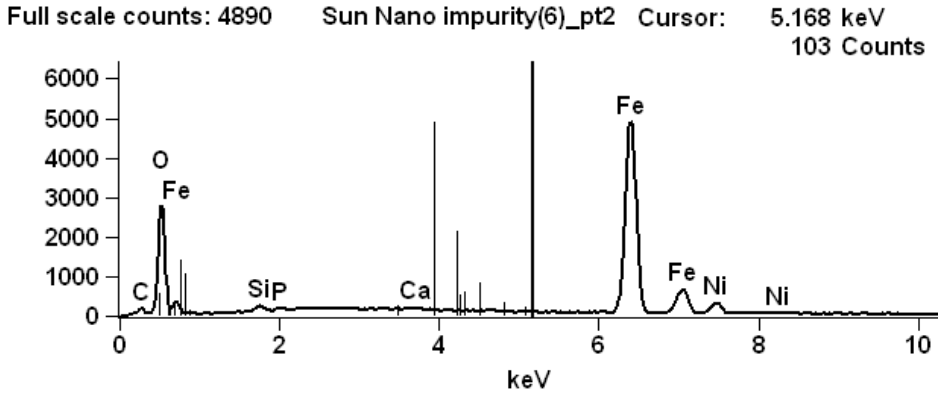

Figure 43- Small Area EDX Scan of Dark Area of the Sample-Showing Nanopit in Dark Material

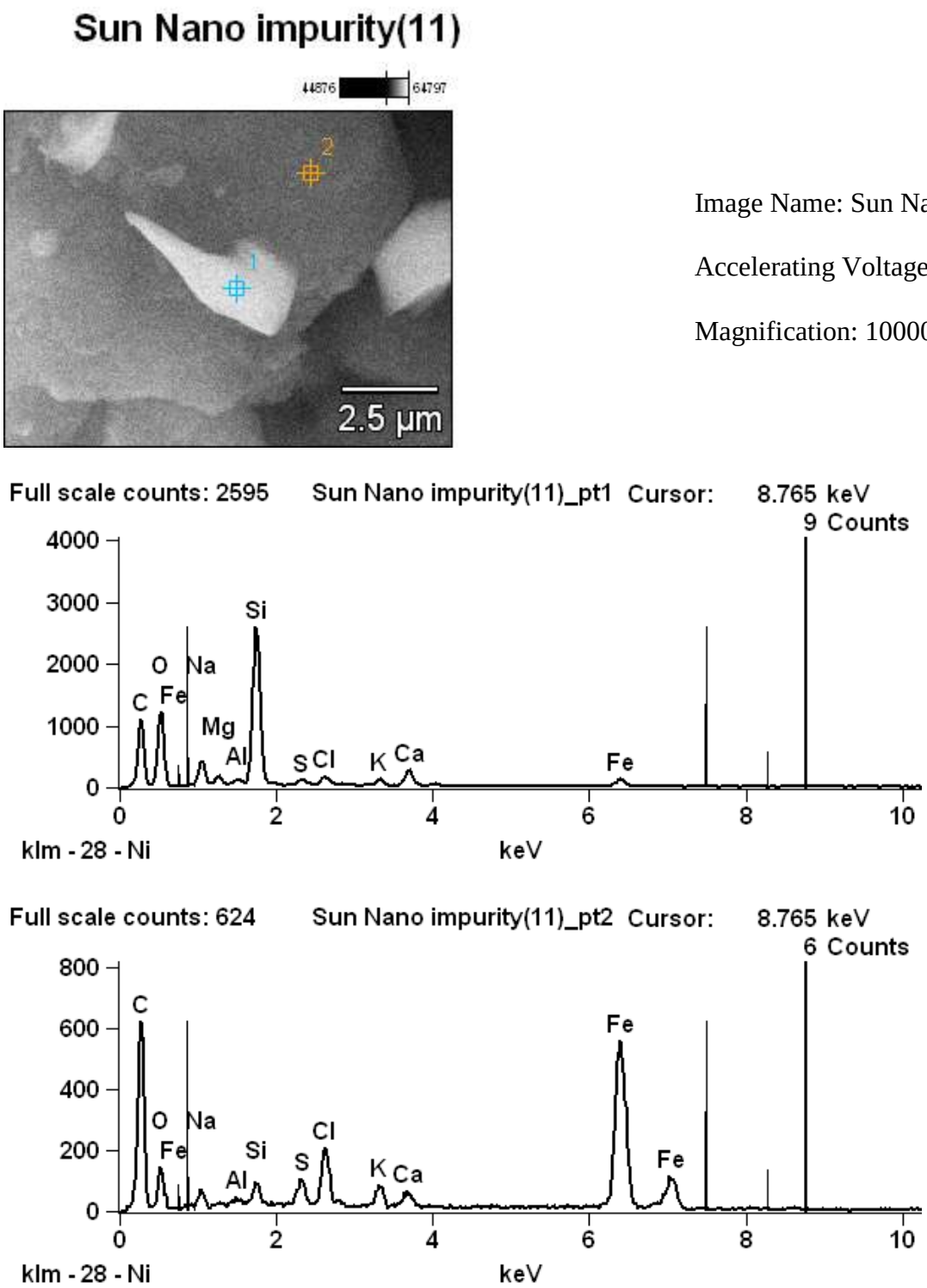

Figure 44- Small Area EDX Scan of Light Area of the Sample-Showing Horn-like Structure

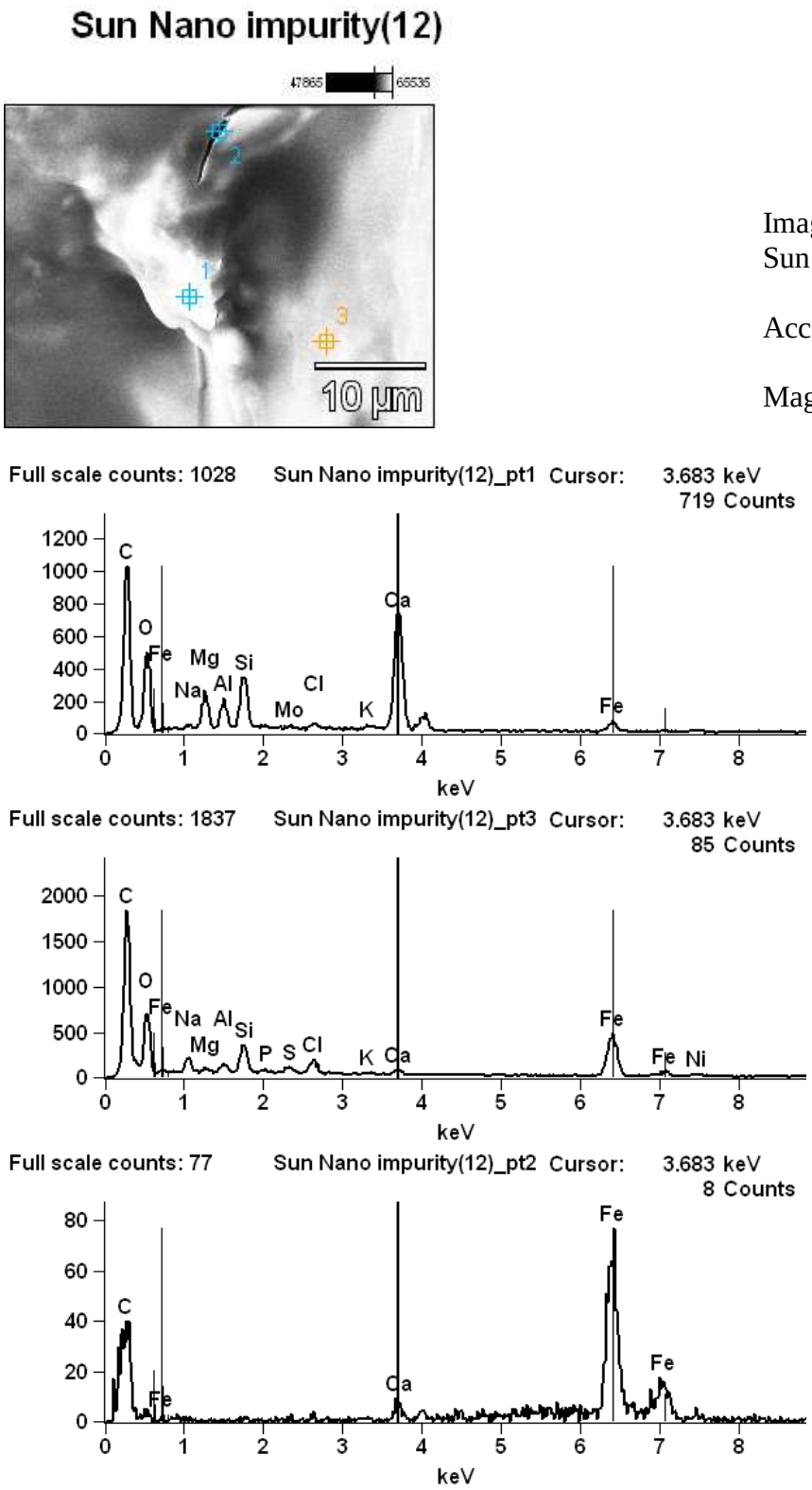

Image Name:
Sun Nano impurity(12)

Accelerating Voltage: 20.0 kV

Magnification: 3000

Figure 45- Small Area EDX Scan of Adjacent Light and Dark Areas of the Sample

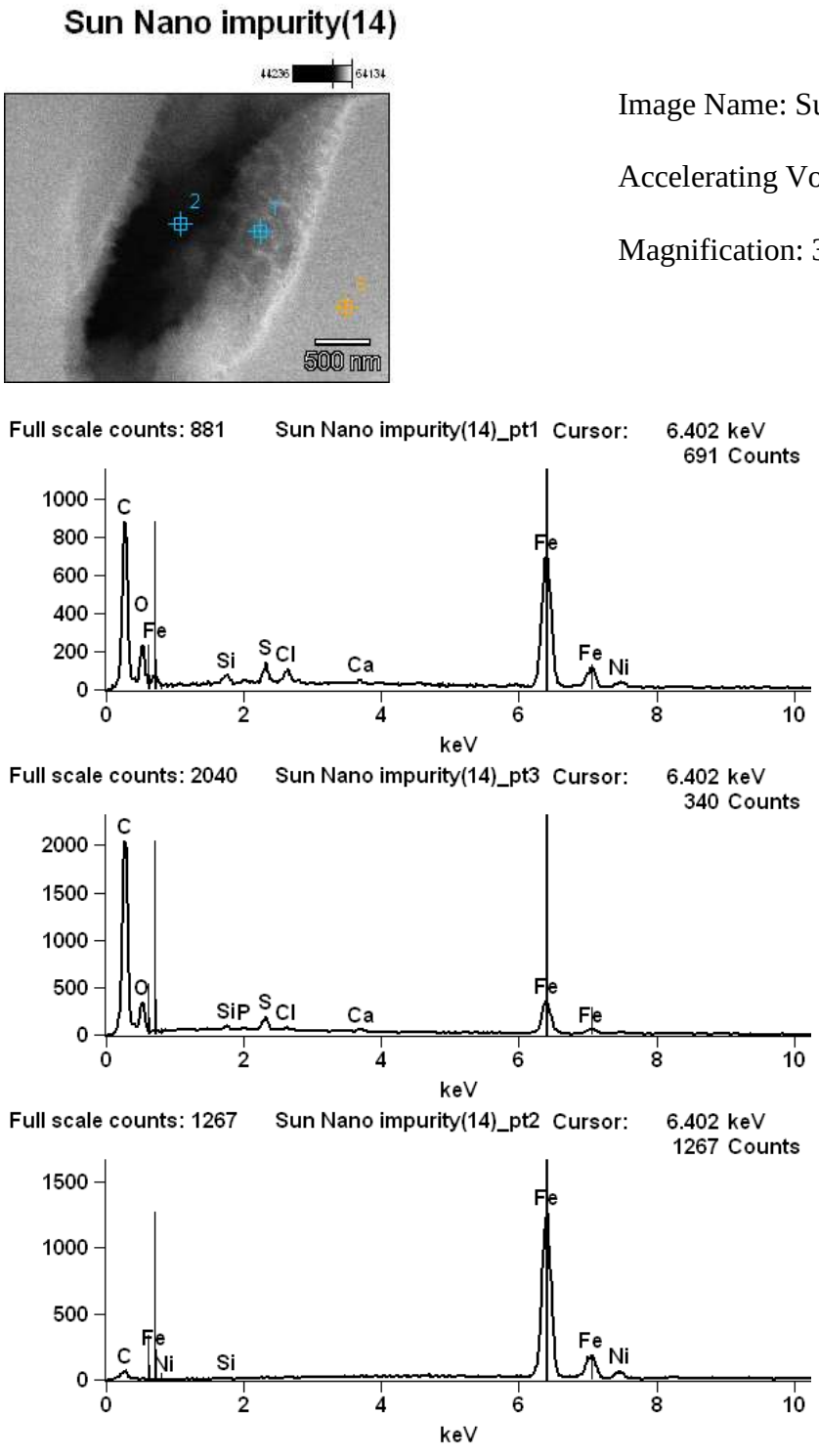

Figure 46- Small Area EDX Scan of Crack in Light Area of the Sample-Showing Nanotubes

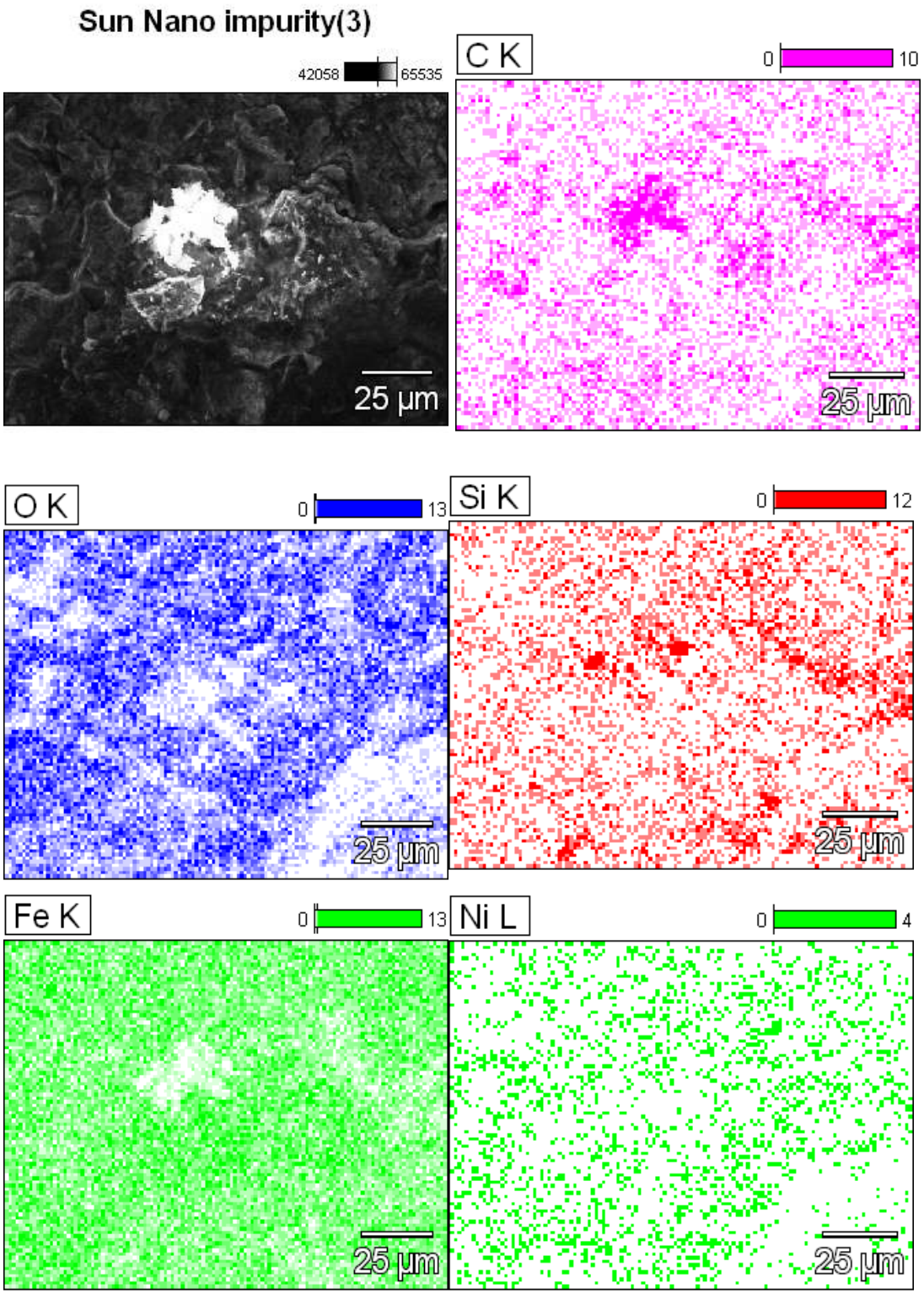

Figure 47–EDX Elemental Mapping of Sample-Showing less Fe and Ni, and more C, O, and Si in Light Colored Inclusion

Data Type: Counts Mag: 750 Acc. Voltage: 20.0 kV

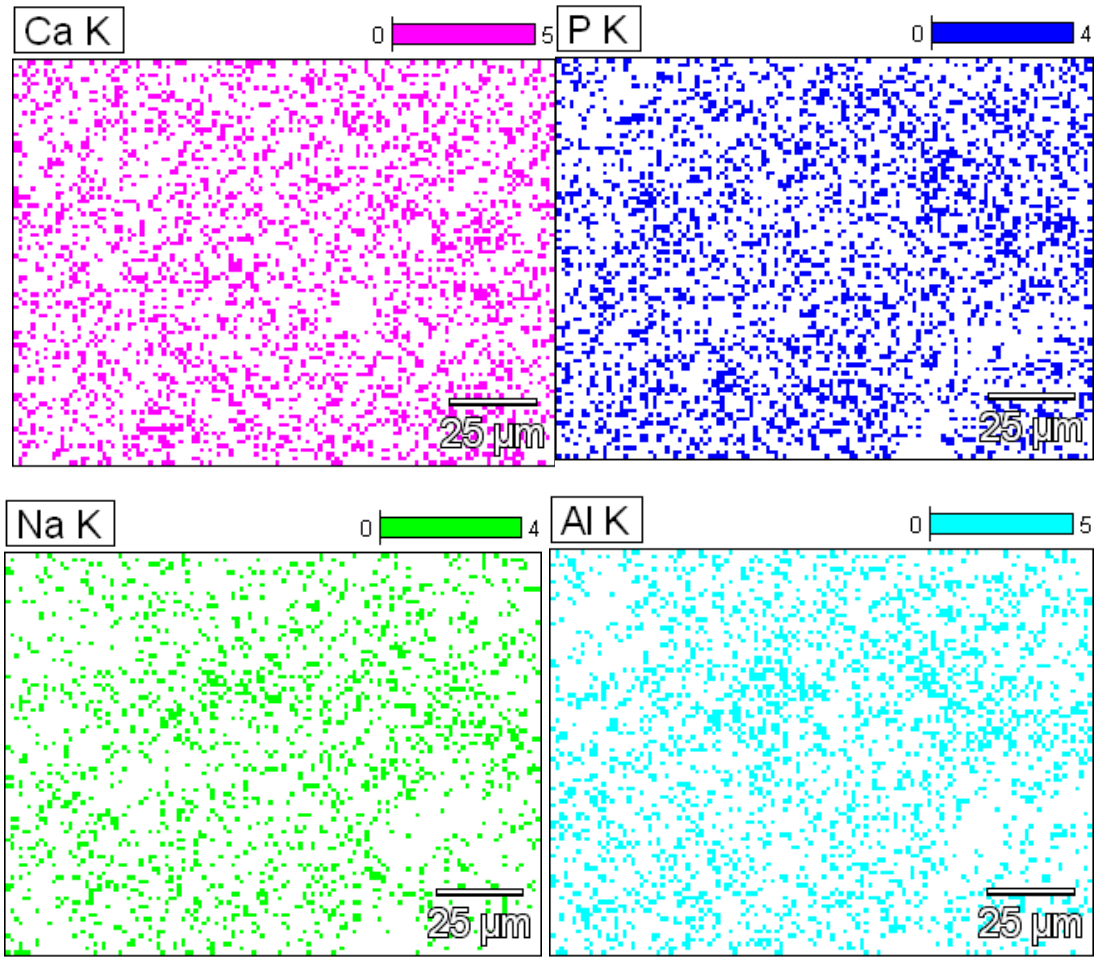

Figure 47 (continued)–EDX Elemental Mapping of Sample-Showing more Na and Al in Light Colored Inclusion

Data Type: Counts Mag: 750 Acc. Voltage: 20.0 kV

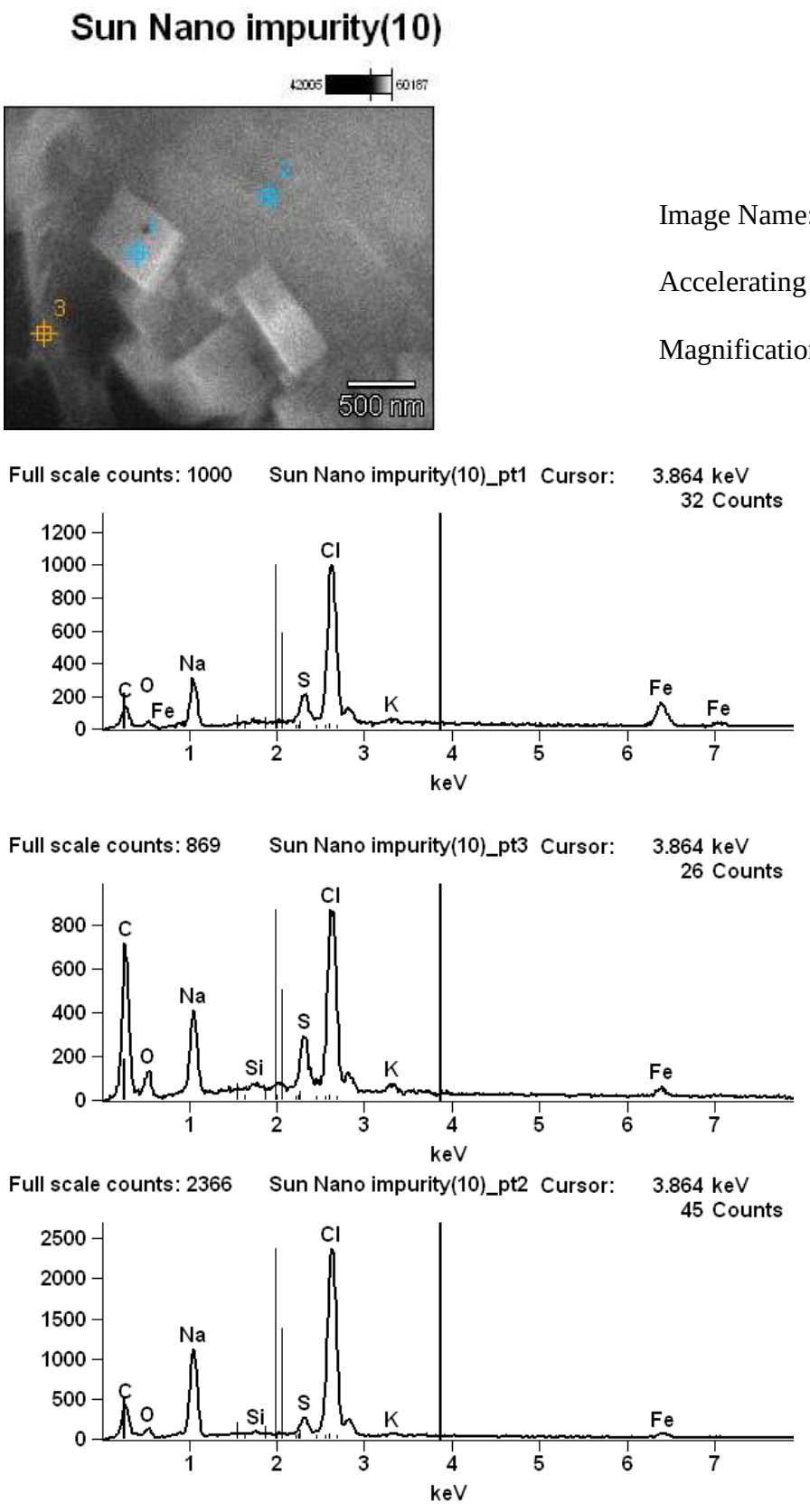

Figure 48- Small Area EDX Scan of Crystals and Adjacent Areas of Sample

An unusual, horn-like, structure was observed (Figure 44), which showed an unusually high concentration of silicon, as compared to the other areas of light material which were imaged.

Small (~500 nm) orthorhombic crystals were also imaged (Figure 48), which were mainly composed of sodium and chlorine, with smaller amounts of sulfur, potassium, and iron. It is likely that the metallic elements in the crystals are present as the chlorides, and sulfates. These crystals were distributed in many locations on the dark material of the sample, and were uniform in size and shape.

EDX elemental mapping of larger areas of the sample (Figure 47), confirms that the composition of the light and dark areas are significantly different, with much more carbon, oxygen, silicon, sodium, and aluminum present in the lighter areas, along with less iron and nickel. Calcium and phosphorus appear to be more uniformly distributed in the sample.

Magnetic Analysis

The sample was found to be strongly attracted to a neodymium-iron-boron (NIB) magnet.

Raman Spectroscopy

The results of the Raman analyses, for 532 nm and 633 nm excitation wavelengths, are shown in Figures 49-51. Raman spectra of the sample are compared to Raman spectra of iron oxide, a sample of iron meteorite, and single-walled carbon nanotubes (SWCNT).

Five of the peaks seen in the low wave-number part of the 532 nm Raman spectrum of the sample (Figure 49, 159 cm^{-1} to 679 cm^{-1}) appear to be a close match to similar peaks seen in the 532 nm Raman spectrum of the sample of iron meteorite[5].

The first and last of these four peaks also appear to roughly match two of the peaks seen in the 532 nm Raman spectrum of the iron oxide sample.

Three very interesting peaks are seen in the high wave-number portion of the 532 nm Raman spectrum of the sample (1312.0 cm^{-1}, 1566.8 cm^{-1}, and 1587.7 cm^{-1}, Figure 50).

These three peaks appear to match the D-band, and both metallic (Met) and semi-conducting (SC) G-band peaks of the 532 nm Raman spectrum of the single-walled carbon nanotube sample. The sample peaks appear up-shifted by approximately 3 cm^{-1}-4 cm^{-1}, relative to the carbon nanotube sample selected for comparison.

If these peaks are produced by the presence of carbon nanotubes, it is likely that the 159 cm^{-1} peak is a carbon nanotube radial breathing mode (RBM) band peak.

[5] This was a sample of the Campo de Cielo iron meteorite, from Argentina.

The 633 nm Raman spectrum of the sample (Figure 51) shows what appear to be the same peaks seen at 532 nm, with somewhat greater intensities for the peaks in the lower wave-number portion of the spectrum. The peak corresponding to the CNT G-Band is somewhat less intense, however.

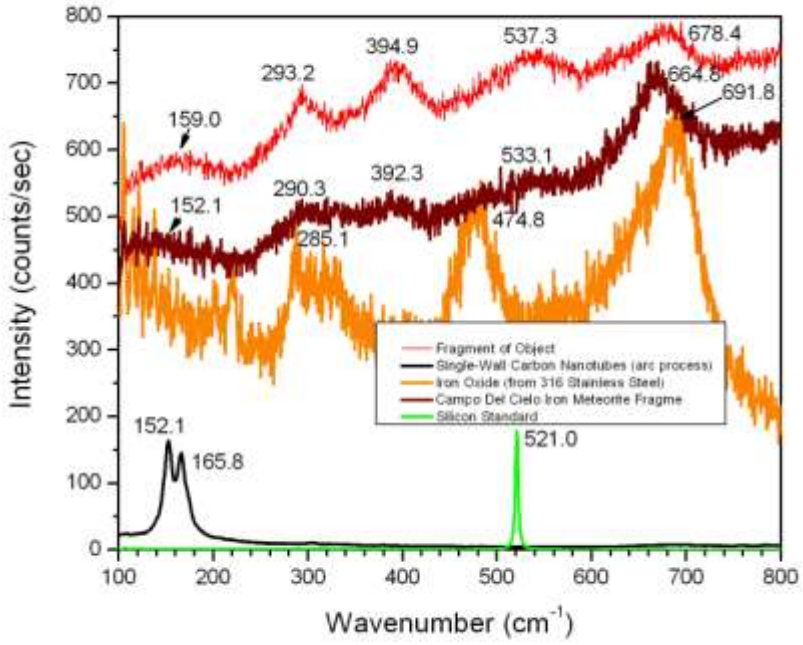

Figure 49-532 nm Raman Spectrum of Sample-as compared to iron oxide, a sample of iron meteorite, and single-walled carbon nanotubes-Low Wave-Numbers

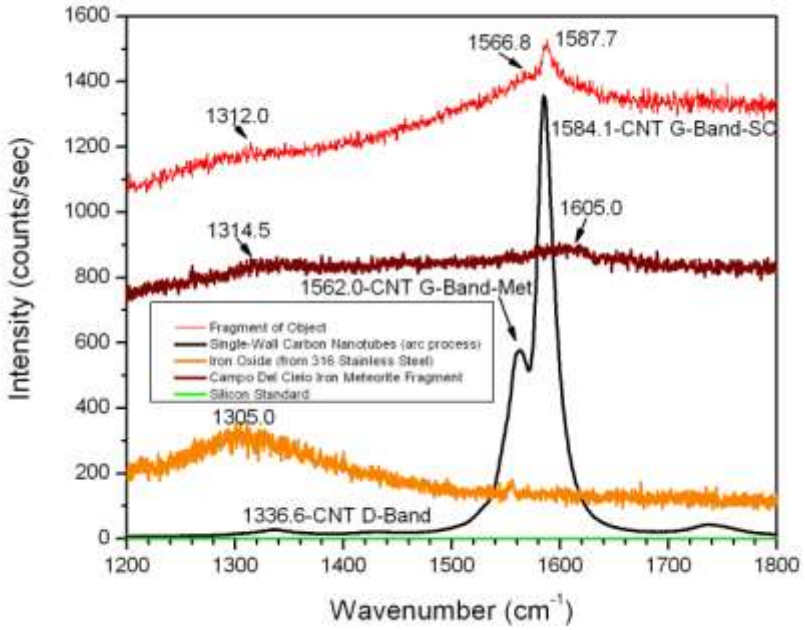

Figure 50-532 nm Raman Spectrum of Sample-as compared to iron oxide, a sample of iron meteorite, and single-walled carbon nanotubes-High Wave-Numbers

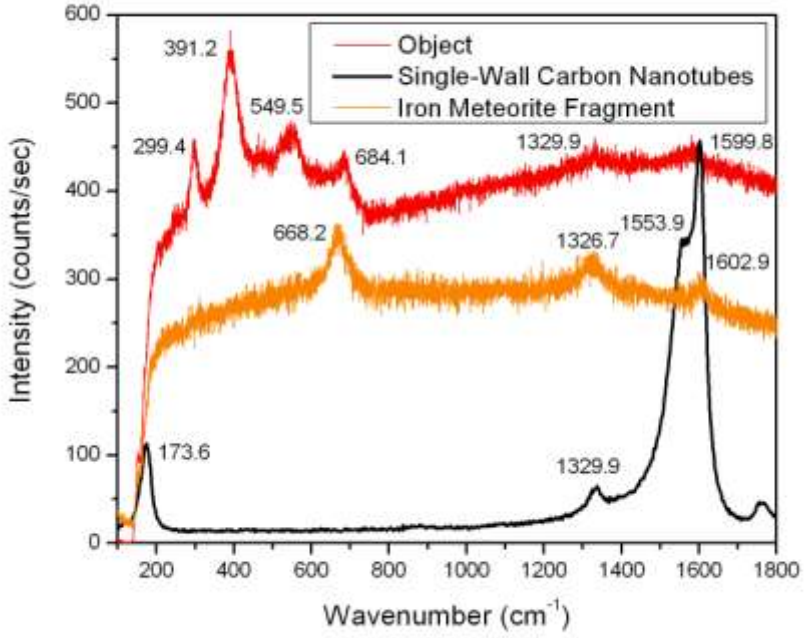

Figure 51-633 nm Raman Spectrum of Sample-as compared to iron oxide, a sample of iron meteorite, and single-walled carbon nanotubes-Full Spectrum

ICP-MS Analysis

An inductively-coupled plasma-mass spectroscopy (ICP-MS) analysis was performed on a piece of the object removed from Mr. Smith, after the SEM, EDX, and Raman data had been obtained. The ICP-MS analysis was performed by an independent laboratory. The piece of the sample used was the same one which was analyzed in the previous tests in this report.

The sample piece was digested in a mixture of nitric and hydrochloric acids[6], and an aliquot of the liquid analyzed by ICP-MS. A portion of the sample, which did not dissolve, proved to contain carbon nanotubes[7].

The ICP-MS elemental analysis confirmed the EDX results, concerning the major components of the sample, and also found many trace elements, which were not detected by EDX (Table 1). A total of fifty one (51) elements were detected in the sample by ICP-MS[8].

The major components of the sample, in order of abundance, were iron (> 46%)[9], and nickel (5.20%).

[6] See bottom of next page for details of the digestion process.
[7] This was shown by Raman analysis of the residue; carbon nanotubes are very resistant to the action of most reactive chemicals, and would be expected to survive this type of acid digestion process.
[8] The ICP-MS analysis was not sensitive to halogens (F, Cl, Br, I), or sulfur (S).
[9] An exact percentage of iron cannot be obtained from this analysis, because the mass spectrometer detector was saturated. The EDX-derived value for the percentage of iron in the sample (~94%) is more accurate, in this case.

Table 1-Results of ICP-MS Analysis of Piece of Implant Sample

Client: A&S Research Inc
Job Number: 110609

Trace Impurities by SOP 7040, Rev 9
Inductively Coupled Plasma - Mass Spectrometry

Sample ID: SN Chunk 080911

	ppm	Detection Limit		ppm	Detection Limit
Aluminum	260	30	Molybdenum	9.3	0.05
Antimony	0.37	0.2	Neodymium	0.39	0.02
Arsenic	17	0.4	Nickel	52000	0.1
Barium	96	0.1	Niobium	0.37	0.1
Beryllium	ND	0.05	Osmium	2.2	0.09
Bismuth	ND	0.03	Palladium	3.3	0.02
Boron	15	3	Phosphorus	1600	10
Bromine	ND	5	Platinum	10	0.02
Cadmium	ND	0.09	Potassium	ND	50
Calcium	1500	30	Praseodymium	0.11	0.02
Cerium	0.85	0.03	Rhenium	0.66	0.02
Cesium	ND	0.02	Rhodium	2.8	0.02
Chromium	13	0.2	Rubidium	0.15	0.02
Cobalt	2200	0.09	Ruthenium	8.0	0.02
Copper	170	0.3	Samarium	0.13	0.02
Dysprosium	0.11	0.02	Selenium	2.5	1
Erbium	0.07	0.02	Silicon	2700	50
Europium	0.03	0.02	Silver	ND	0.02
Gadolinium	0.13	0.02	Sodium	230	10
Gallium	130	0.02	Strontium	10	0.2
Germanium	300	0.1	Tantalum	ND	0.07
Gold	0.90	0.09	Tellurium	ND	0.1
Hafnium	0.10	0.02	Thallium	ND	0.2
Holmium	ND	0.02	Thorium	0.23	0.02
Iodine	ND	0.9	Thulium	ND	0.02
Iridium	3.6	0.05	Tin	6.5	0.1
Iron	460000	4	Titanium	20	0.3
Lanthanum	ND	1	Tungsten	1.9	0.07
Lead	1.3	0.1	Uranium	0.21	0.02
Lithium	ND	1	Vanadium	21	1
Lutetium	ND	0.5	Ytterbium	0.05	0.02
Magnesium	890	5	Yttrium	0.88	0.4
Manganese	62	0.1	Zinc	44	2
Mercury	ND	0.1	Zirconium	4.4	0.3

Note: the entire sample (0.0058 g) was mixed with 0.5 mL nitric acid and 0.5 mL hydrochloric acid and heated on a hotblock set at 110°C for 1 hour. The mixture was cooled, 0.5 mL 30% hydrogen peroxide added, and heated 30 min. A portion remained undissolved; therefore, silicon or other elements that have low solubility in this acid mixture may be biased low. The solution was mixed with internal standards, diluted to 10 g, and a 1:100 dilution also analyzed by ICPMS.

Date Analyzed: 11-26-08

Elements Not Analyzed: All Gases, C, S, Sc, In, Tb

Minor component elements, in order of abundance (Table 2), were silicon (0.27%), cobalt (0.22%), phosphorus (0.16%), and calcium (0.15%).

Table 2-Elements Detected in Implant Sample by ICP-MS-in Order of Abundance

Element[10]	Amount (ppm)	Detection Limit (ppm)	Element	Amount (ppm)	Detection Limit (ppm)
Iron	> 460000	4	Gold	0.90	0.09
Nickel	52000	0.1	Yttrium	0.88	0.4
Silicon	2700	50	Cerium	0.85	0.03
Cobalt	2200	0.09	Rhenium	0.66	0.02
Phosphorus	1600	10	Neodymium	0.39	0.02
Calcium	1500	30	Niobium	0.37	0.1
Magnesium	890	5	Antimony	0.37	0.2
Germanium	300	0.1	Thorium	0.23	0.02
Aluminum	260	30	Uranium	0.21	0.02
Sodium	230	10	Rubidium	0.15	0.02
Copper	170	0.3	Samarium	0.13	0.02
Gallium	130	0.02	Gadolinium	0.13	0.02
Barium	96	0.1	Dysprosium	0.11	0.02
Manganese	62	0.1	Praseodymium	0.11	0.02
Zinc	44	2	Hafnium	0.10	0.02
Vanadium	21	1	Erbium	0.07	0.02
Titanium	20	0.3	Ytterbium	0.05	0.02
Arsenic	17	0.4	Europium	0.03	0.02
Boron	15	3			
Chromium	13	0.2			
Strontium	10	0.2			
Platinum	10	0.02			
Molybdenum	9.3	0.05			
Ruthenium	8.0	0.02			
Tin	6.5	0.1			
Zirconium	4.4	0.3			
Iridium	3.6	0.05			
Palladium	3.3	0.02			
Rhodium	2.8	0.02			
Selenium	2.5	1			
Osmium	2.2	0.09			
Tungsten	1.9	0.07			
Lead	1.3	0.1			

[10] Red denotes major component elements (100%-1%), green-minor component elements (10,000 ppm-1,000 ppm) blue-major trace elements (1,000 ppm-100 ppm), black-minor trace elements (< 100 ppm).

Major trace elements detected included magnesium (890 ppm, or 0.089%), germanium (300 ppm), aluminum (260 ppm), sodium (230 ppm), copper (170 ppm), and gallium (130 ppm).

Minor trace elements included boron (15 ppm), barium (96 ppm) and strontium (10 ppm), titanium (20 ppm), vanadium (21 ppm), chromium (13 ppm), manganese (62 ppm), zinc (44 ppm), and arsenic (17 ppm).

The sample also contained smaller amounts of precious metals, including platinum (10 ppm), ruthenium (8.0 ppm), iridium (3.6 ppm), palladium (3.3 ppm), rhodium (2.8 ppm), osmium (2.2 ppm), and gold (0.90 ppm).

Other transition elements present included molybdenum (9.3 ppm) and tungsten (1.9 ppm), tin (6.5 ppm), zirconium (4.4 ppm) and hafnium (0.10 ppm), yttrium (0.88 ppm), rhenium (0.66 ppm), and niobium (0.37 ppm).

The sample also contained traces of rare earth elements, and actinides. The rare earth elements detected included cerium (0.85 ppm), neodymium (0.39 ppm), samarium (0.13 ppm), gadolinium (0.13 ppm), dysprosium (0.11 ppm), praseodymium (0.11 ppm), erbium, (0.07 ppm), ytterbium (0.05 ppm), and europium (0.03 ppm). Actinides detected included thorium (0.23 ppm), and uranium (0.21 ppm).

The remaining trace elements detected included selenium (2.5 ppm), lead (1.3 ppm), antimony (0.37 ppm), and rubidium (0.15 ppm).

Potassium was not detected in the ICP-MS analysis, although it was detected in the sample by EDX. It is likely that the amount of potassium in the sample was below the detection limit of the ICP-MS analysis (50 ppm).

Isotopic Analysis

The raw ICP-MS data had sufficient resolution to calculate percentages of isotopes for four of the elements detected in the sample (boron, magnesium, nickel, and copper).

The distribution of isotopes in the elements the sample is made of is a strong indication of the area that the sample was formed. Any deviation of more than 1% of the isotopic ratios in the sample from the terrestrial isotopic distribution indicates that the sample was probably not formed on Earth.

The data showed significant differences between the isotopic distributions of most of the sample elements, for which isotopic data was available, and the isotopic distributions of the same elements obtained from Earthly sources.

The isotopic distributions of the elements in the sample differed by as much as 4% from the terrestrial distributions of the same elements, indicating that the sample probably did not originate on Earth.

Table 3-Isotopic Abundances of Elements Detected in Implant Sample

Isotope	Sample Isotopic Abundance (%)	Terrestrial Isotopic Abundance (%)	Error (%)
Sb^{121}	49.68	57.36	3.6
Sb^{123}	50.32	42.64	5.7
B^{10}	54.24	19.9	12.2
B^{11}	45.76	80.1	9.0
Mg^{24}	49.61	78.99	1.2
Mg^{25}	Mg^{25} and Mg^{26} 50.39	10.00	1.2
Mg^{26}		11.01	0.2
Ni^{58}	29.13	68.08	NS
Ni^{60}	35.03	26.23	1.0
Ni^{61}	0	1.14	NS
Ni^{62}	35.84	3.63	1.0
Ni^{64}	0	0.93	NS
Cu^{63}	49.74	69.15	1.4
Cu^{65}	50.26	30.85	2.1

Discussion

The iron/nickel metal matrix which made up the majority of the sample which was analyzed bore a strong resemblance to an iron-nickel meteorite.

This is seen by the similarity of the light microscope images of the sample to those of an iron meteorite sample, by the traces of iridium and tungsten seen in the EDX analysis, and by the similarity of the Raman spectrum of the sample to that of a sample of the Campo del Cielo iron-nickel meteorite.

The resemblance of the sample to a meteorite was confirmed by the pattern of trace elements detected in the ICP-MS analysis. The analysis confirmed the presence of traces of iridium, which is very rare on earth, but is universally present in meteoric iron.

The analysis also showed the presence of relatively large amounts of gallium (130 ppm) and germanium (300 ppm), which are also generally present in iron-nickel meteorites, at concentrations of up to 100 ppm for gallium (Ga), and up to 400 ppm for germanium (Ge). These concentrations of Ga and Ge would therefore be considered to be at the high end of the concentration range for these elements, in an iron-nickel meteorite.

The presence of traces of precious metals, other than iridium, is also a good indicator of possible meteoric origin of the metallic portion of the sample. The elements carbon (C), copper (Cu), cobalt (Co), sulfur (S), phosphorus (P), chromium (Cr), gallium (Ga), germanium (Ge), arsenic (As), antimony (Sb), tungsten (W), rhenium (Re), iridium (Ir), gold (Au), ruthenium (Ru), palladium (Pd), osmium (Os), praseodymium (Pr), and

manganese (Mn) have all been detected in iron-nickel meteorites. All of these elements were also detected in the ICP-MS analysis of the sample from Mr. Smith's toe.

If the sample matrix material is derived from meteoric iron, its nickel content (5.2%, by ICP-MS, 6% by EDX) is somewhat low, but within the range of nickel percentages published in the literature (5%-25%), for known iron-nickel meteorites. This concentration of nickel would place the material in a class of low-nickel iron meteorites, known as hexahedrites.

The differences in the isotopic ratios of the sample elements from those which are observed in elements derived from terrestrial sources were quite remarkable, and cannot be easily explained, except by an extraterrestrial origin of the sample material.

Isotopic percentages in elements derived from terrestrial sources have not been observed to vary by more than ±1%, at most, while the variations in the percentages of isotopes observed in many of the sample elements were more than 2X greater than this.

Some lighter isotopes of meteoric origin, such as boron, have been observed to vary in isotopic percentages by up to 19%, relative to the same elements derived from terrestrial sources. Heavier elements from known meteorites[11] have not been observed to vary in isotopic abundances, with respect to terrestrial standards, by nearly as much as was observed in all of the elements which were analyzed for isotopic distribution in the ICP-MS test of the current sample.

This could indicate that the material is not only extraterrestrial, but may originate from a different solar system than our own. The point of origin of the sample material may perhaps lie nearer the center of our galaxy, where supernovae[12] are more common.

The high percentage of iron observed in the chemical analysis data indicates strongly that the red patina on the sample, as delivered, was hydrated iron oxide (rust), a corrosion product formed by contact of the iron in the sample with oxygen, and the water present in the blood serum the sample was stored in. The salts dissolved in the blood serum undoubtedly accelerated the corrosion of the metallic portion of the sample.

The black material, seen on the sample pieces by Dr. Leir, soon after removal from the patient, was freshly formed iron oxide[13], in which hydration had not yet been completed.

The sample had an outer coating of a non-metallic, ceramic-like material, which was approximately 100 nm-200 nm in thickness. This material had a somewhat rough texture, as seen under SEM, with surface irregularities up to several microns in size.

---

[11] Isotopic analyses of iron meteorite trace elements were found in the literature for Ni, Pt, Pd, Os, and Rh.
[12] Supernovae create heavy elements by the r (rapid) process of neutron-capture nucleosynthesis. Neutron-rich isotopes of heavy elements are thought to form in supernova explosions.
[13] This material (Fe_2O_3) is black in color, and turns red after long exposure to water.

Large numbers of inclusions of what appeared to be the same material[14], which were typically several microns in size, were also seen in the metallic phase.

The high concentration of non-metallic inclusions in the metallic phase probably account for the brittleness of the original object. Inclusions of unlike material, in this size range, which do not bind well with the sample matrix, act as points of stress concentration during episodes of mechanical stress, which leads to cracking at much lower stress levels than would be the case with a homogeneous metallic material.

The presence of these inclusions is the most likely cause of the breakage of the original object into small pieces, during its removal from Mr. Smith's toe.

The non-metallic, ceramic-like, material contains mainly carbon (C), oxygen (O), silicon (Si), sulfur (S), aluminum (Al), calcium (Ca), iron (Fe) and nickel (Ni), with smaller amounts of sodium (Na), phosphorus (P), chlorine (Cl), potassium (K), and titanium (Ti), and chemically resembles a biological hard part, such as shell, or bone[15].

This similarity of the composition of the non-metallic phase to biological material may be responsible for the lack of immune response to the object by the patient's body.

The opalescence of this material, seen in the light microscopy images, indicates the presence of an organized, layered, structure, such as occurs in mother-of-pearl, or opal, which reflects and refracts light strongly into different color bands.

The Raman data, showing what appears to be carbon nanotube D-Band and G-Band signals, along with a possible radial breathing mode signal, strongly indicates the presence of carbon nanotubes (CNTs). This is confirmed by the SEM images, which show bundles of nanotubes, with high carbon content (EDX data), which appear nearly identical to SEM images of commercial arc-process, single-walled, CNTs.

The data therefore indicates that the majority of the non-metallic phase material is probably composed mainly of carbon nanotubes, which are covered, and/or filled, by a shell-like coating of aluminum, calcium, iron, nickel, and titanium silicates, oxides, sulfates, and phosphates.

A smaller percentage of the non-metallic phase of the sample is composed of the very regularly sized (500 nm), and shaped, sodium, potassium, and iron, chloride and sulfate-containing crystals, seen in the SEM images. These crystals appear to be far too regular in size and shape to have formed spontaneously, from drying of the salts in the blood serum the samples was stored in.

The shapes of the inclusions of the lighter, non-metallic, material in the Fe/Ni phase appear to be non-random, such as the long bone-like, and horn-like structures seen in the

[14] EDX elemental analyses of the inclusions and the outer coating were very similar.
[15] Elemental composition of the non-metallic, ceramic-like phase of the sample was derived from EDX data.

SEM images. The Fe/Ni phase also has numerous pits, of regular size (400 nm-500 nm) and shape.

The carbon nanotubes inside the above structures would be excellent carriers of electric current, and could also act as electronic components, depending on whether the CNT type were metallic, or semiconducting. The shell-like coating on the material would then provide good electrical insulation for these nano-components.

The relatively large amounts of silicon and germanium in the sample may also be indicative of the presence of silicon-based, and/or germanium-based electronic components in the sample.

It is not likely that inclusions of the type observed could have formed within molten iron/nickel, during the formation process of an iron-nickel meteorite, since the solubilities of most ceramics in molten iron is high enough to dissolve a small percentage of ceramic inclusions, especially if these were small in size. It is also difficult to conceive of a natural process in which ceramic inclusions of this type could be formed inside metal, while the metal is in the solid state.

There are, in any event, no known meteorites which contain ceramic inclusions of this type. This is an anomaly, considering the fact that all the other evidence appears to point to a meteoric origin for the sample.

Because of this observation, the observation that the inclusions appear to be artificially shaped nano-components, and the fact that the complete object was giving off radio signals, before removal, the conclusion is inescapable that the object the sample came from is a manufactured item, which was made using extraterrestrial materials, by an organization possessing a high degree of technological sophistication.

The differently shaped inclusions of the non-metallic, CNT-containing material could then be for the performance of different functions in the device, such as carrying electric current (bone-like structures), acting as antenna for emitting, or receiving, radio signals (horn-like structures), or acting as resonators, to generate the radio waves (salt-containing crystals).

The magnetic nature of the metallic matrix material of the object may be necessary for the object, or device, to function, or, alternatively, meteoric iron could have been chosen as a base material simply because of its abundance in our solar system, and probably other solar systems, as well.

This would make it a relatively inexpensive material for use in manufacture, if the organization, or society, that made the object already had inexpensive methods of space transport, and travel.

The manufacture of a device comparable to this one is probably beyond the technology of known, Earthly, commercial processes, at the present time. It is most likely, therefore,

that the device was manufactured by an alien civilization. It is still a possibility, however, that the device was manufactured by some process known to the Earthly military/Black Project community.
The hypothesis that this sample came from a manufactured, nanotechnological device should be investigated by further research on this, and all other such samples, obtained previously.

Further research should include include Raman analysis, to check for the presence of carbon nanotubes in the older samples, and their analysis by ICP-MS.

One, or more, samples should also be subjected to a combination of SEM imaging, EDX elemental analysis, and etching by fast-atom bombardment. This type of technique should allow a layer by layer, three dimensional, image to be built up of the composition of the sample. This type of information may be essential to understanding of the function of these devices. Study of the electrical characteristics of these samples may also be of great benefit.

Conclusions

1. The sample consists mainly of iron, with a high carbon and oxygen content. The iron base material contains 5.2% nickel, and is highly magnetic. Traces of iridium, and other precious metals, tungsten, gallium, and germanium present strongly suggest that the metallic portion of the sample was derived from meteoric iron, and is extraterrestrial in origin.
2. The extreme differences in the isotopic ratios of the sample elements from the isotopic ratios of elements found on Earth provide strong confirmation that the material in the sample is of extraterrestrial origin.
3. The sample consists of two major phases; an iron/nickel (Fe/Ni) phase, and a non-metallic phase resembling a hard biological substance, such as shell, tooth, or bone. The iridescence of the non-metallic phase, seen in light microscopy, suggests a layered microstructure, perhaps similar to mother-of-pearl, or opal.
4. The similarity of the composition of the non-metallic phase to biological material may be responsible for the lack of immune response to the object by the patient's body.
5. This non-metallic phase is high in carbon, oxygen, silicon, magnesium, aluminum, sulfur, and phosphorus, and is present as an outer covering on the sample, and as inclusions in the metallic, Fe/Ni phase.
6. The non-metallic phase of the sample also contains bundles of carbon nanotubes, perhaps covered, or filled, with calcium and magnesium silicates, phosphates and sulfates.
7. The inclusions of the non-metallic phase have unusual shapes, which suggest artificiality, and functionality. This, along with the fact that the object was giving off radio signals, before removal, strongly indicates that this is a manufactured, nanotechnological device, which was inserted in patient Smith for a definite purpose.

8. The function of the device cannot be determined with certainty from the available data, and the device may have had multiple functions and missions. It is likely, however, that two of its functions had to do with monitoring of the physiological state of Mr. Smith's body, and mood/mind control.

Bibliography

Lithium Isotope Analysis of Inorganic Constituents of the Murchison Meteorite-Mark A. Sephton, et. al.; The Astrophysical Journal, 612:588-591, September 1, 2004

Boron Isotope Ratios in Meteorites and Lunar Rocks-Zhai, et. al., Geochimica et Cosmochimica Acta, vol. 60, Issue 23, 12/1996, pp.4877-4881

Carbon Isotope Abundance in Meteoritic Carbonates-Robert N. Clayton; Science, 12 April (1963) pp. 192-193

Ti^{50} Anomalies in Primitive and Differentiated Meteorites-Goldschmidt Conference Abstracts, A1038 (2007)

Measurements of the Isotopic Ratios of Nickel in Iron Meteorities, Using Nickel Carbonyl-Masaru Suzuki and Sadao Matsuo; Geochemical Journal, vol. 1, pp. 50-60, 1967

Nickel Isotope Anomalies in Meteorites and the Fe^{60}-Ni^{60} Clock-M. Bizzarro, et. al.; Workshop on Chronology of Meteorites (2007)

Germanium Isotopic Fractionation in Iron Meteorites-64^{th} Annual Meteoritical Society Meeting (2001)

Tungsten Isotope Evidence from 3.8-Gyr Metamorphosed Sediments for Early Meteorite Bombardment of the Earth-Shoenberg, et. al.; Nature 418, 403-405 (25 July 2002)

Tungsten Isotopic Constraints on the Formation and Evolution of Iron Meteorite Parent Bodies-A. Markowski, et. al.; Dept. of Earth Sciences, Oxford Univ.; Lunar and Planetary Science XXXVI (2005)

Microanalysis of Platinum Group Elements in Iron Meteorites Using Laser Ablation ICP-MS- A. J. Campbell and M. Humayun, Dept. of Geophysical Sciences, Univ. of Chicago; Lunar and Planetary Science XXX (1974)

New Applications of the Re187-Os187 and Pt190-Os186 Systems to the Study of Iron Meteorites-D. L. Cook, et. al., Isotope Geochemistry Laboratory, Dept. of Geology, Univ. of Maryland; Lunar and Planetary Science XXXI

Compilation of Minimum and Maximum Isotope Ratios of Selected Elements in Naturally Occurring Terrestrial Materials and Reagents-Coplen, et. al.; U.S. GEOLOGICAL SURVEY Water Resources Investigation Report 01-4222

Meteorites: A Petrologic, Chemical and Isotopic Synthesis-Cambridge Planetary Science Series-R. Hutchinson; Cambridge University Press (2004)